Journal of Structural Geology 96 (2017) 1–20

Contents lists available at ScienceDirect

Journal of Structural Geology

journal homepage: www.elsevier.com/locate/jsg

Analysis of transpression within contractional fault steps using finite-element method

Seyed Tohid Nabavi [a, *], Seyed Ahmad Alavi [a], Soheil Mohammadi [b], Mohammad Reza Ghassemi [c], Marcel Frehner [d]

[a] Faculty of Earth Sciences, Department of Geology, Shahid Beheshti University, Tehran, Iran
[b] High Performance Computing Laboratory, School of Civil Engineering, University of Tehran, Tehran, Iran
[c] Research Institute for Earth Sciences, Geological Survey of Iran, Tehran, Iran
[d] Geological Institute, NO E3, ETH Zürich, Sonneggstrasse 5, Switzerland

ARTICLE INFO

Article history:
Received 15 November 2016
Received in revised form
4 January 2017
Accepted 18 January 2017
Available online 21 January 2017

Keywords:
Transpression
Strike-slip fault
Fault segment
Contractional step
Finite-element method

ABSTRACT

Two-dimensional finite-element modelling of elastic Newtonian rheology is used to compute stress distribution and strain localization patterns in a transpression zone between two pre-existing right-stepping, left-lateral strike-slip fault segments. Three representative fault segment interactions are modelled: underlapping, neutral, and overlapping. The numerical results indicate that at the onset of deformation, displacement vectors are oblique to the regional compression direction (20–90°). The orientations of the local σ_1 (the maximum compressive stress) and σ_3 (the minimum compressive stress) directions strongly depend on the structural position within the transpression zone. For neutral and overlapping fault steps, there is a contractional linking damage zone between the fault segments. For overlapping faults, the σ_1 trajectories within the transpression zone deflects significantly forming a sigmoidal pattern, which is created by two rotational flow patterns close to the fault tips. These flow patterns are related to friction effects and different shear deformation, from pure shear outside of the fault steps toward simple shear along the fault segments. Interaction between the two fault segments perturbs the stress field and reflects the heterogeneous nature of deformation. A lozenge- (for underlapping steps), rhomboidal- (for neutral steps), and sigmoidal-shaped (for overlapping steps) transpression zone developed between the two segments. The modelled mean stress pattern shows a similar pattern to that of the contractional steps, and decrease and increase in underlapping and overlapping fault steps, respectively. Comparison of the Kuh-e-Hori transpression zone, between the Esmail-abad and West Neh left-stepping right-lateral strike-slip fault segments in SE Iran, with the modelling results shows strong similarities with the neutral step configuration.

1. Introduction

On geological maps, strike-slip fault systems are often apparently linear and relatively continuous (Dasgupta and Mukherjee, 2016). However, in nature they are typically discontinuous and segmented on various scales. Such sub-parallel discontinuous fault segments often exhibit en-échelon, non-coplanar geometries and include steps and bends in the master fault that demarcate the boundaries of the strike-slip zones. The individual fault segments are separated from each other and interact through their stress/strain fields. The movement on the fault segment parallel each other and initiates shear fracture/fault (Segall and Pollard, 1983; Pollard and Segall, 1987; Aydin et al., 2006). The represent stepovers between two fault segments represent the locations of extensional or contractional heterogeneous deformations depending on the sense of fault step with respect to the sense of slip along the main strike-slip fault system (Fig. 1). The sense of step is described as left- and right-stepping. Releasing or extensional stepovers result where the sense of step is the same as the sense of the overall slip (e.g., a left-step along a left-lateral fault) (Biddle and Christie-Blick, 1985; Christie-Blick and Biddle, 1985; Woodcock and Fischer, 1986; Sylvester, 1988; Woodcock and Schubert, 1994; Westaway, 1995; Cunningham and Mann, 2007; Mann, 2007; Crider, 2015; Cao and Neubauer, 2016; Kattenhorn et al., 2016;

* Corresponding author.
E-mail addresses: Tohidnabavi@gmail.com, T_nabavi@sbu.ac.ir (S.T. Nabavi).

http://dx.doi.org/10.1016/j.jsg.2017.01.004
0191-8141/

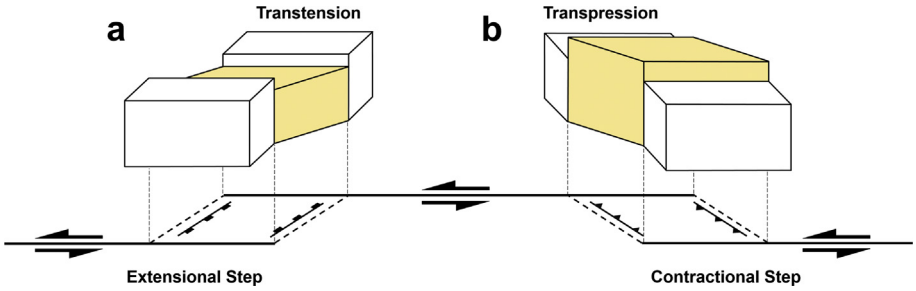

Fig. 1. Typical relation of the geometry of **a** extensional and **b** contractional steps along a left-lateral strike-slip faults to block diagrams of **a** transtension and **b** transpression.

Peacock et al., 2016); related structures include open and dilatant cracks at cm to m-scale (e.g., Segall and Pollard, 1980, 1983; Martel et al., 1988; Kim et al., 2000, 2003, 2004; Flodin and Aydin, 2004) and pull-apart basins, sag ponds and negative flower structures (e.g., Mann et al., 1983; Aydin and Nur, 1985; Mukherjee, 2015a, 2015b). However, all these structures need not form in every strike-slip settings (Misra et al., 2014, 2015, 2016; Misra and Mukherjee, 2015, in press-1, in press-2; Babar et al., in press; Kaplay et al., in press, submitted; Mukherjee et al., in press). In contrast, restraining or contractional stepovers, or contractional linking damage zone (Kim et al., 2004), result where the sense of step is opposite to the sense of the overall slip (e.g., a right-step along a left-lateral fault or vice versa) (Biddle and Christie-Blick, 1985; Christie-Blick and Biddle, 1985; Woodcock and Fischer, 1986; Sylvester, 1988; Woodcock and Schubert, 1994; Westaway, 1995; Cunningham and Mann, 2007; Mann, 2007; Crider, 2015; Kattenhorn et al., 2016; Peacock et al., 2016); related structures include closing, anti-cracks and pressure solution seams at the m-scale (e.g., Bürgmann and Pollard, 1992, 1994; Peacock and Sanderson, 1995) and pop-up and positive flower structures at the regional scale (e.g., Aydin and Nur, 1985). Contractional fault steps, which are common features of active intra-continental strike-slip fault systems, are commonly referred to as sites of "transpression" (e.g., Curtis, 1997, 1999; McClay and Bonora, 2001; Dooley and Schreurs, 2012). Depending on the assumed fault plane orientation, the extensional and contractional steps may be classified as either "transtension" (Fig. 1a) or "transpression" (Fig. 1b), respectively (Fig. 1). Transpression results in a combination of simple- and pure-shear components (Sanderson and Marchini, 1984; Fossen and Tikoff, 1993, 1998; Fossen et al., 1994; Mukherjee and Koyi, 2010a; Fossen et al., 2013) and related structures (Mukherjee, 2010a, 2013a, 2013b, 2015a, 2015b) on the wide variety of scales from lithospheric plate downwards in any strike-slip zone that is not perfectly planar. Hence transpression zones (non-Andersonian case) can be related to the boundary conditions and obliquity between the imposed compressive stress and plate boundaries (Upton and Koons, 2007; Mukherjee and Koyi, 2010b; Mukherjee, 2012a, 2012b; Fernández et al., 2013; Díaz-Azpiroz et al., 2014; Mukherjee, 2014a, 2014b; Mukherjee and Biswas, 2014, 2015; Díaz-Azpiroz et al., 2016; Frehner, 2016a, 2016b; Nabavi et al., 2016a, 2016b; Philippon and Corti, 2016; Zanchi et al., 2016).

Real geometries of contractional strike-slip fault steps, however, vary more due to the initial separation and increasing offset of faults segments (e.g., Rodgers, 1980; Mann et al., 1983). Numerous field studies (Bürgmann and Pollard, 1994 as for example), analytical studies (Pollard and Segall, 1987 as for example), analog modelling studies (McClay and Bonora, 2001; Dooley and Schreurs, 2012; González et al., 2012; Cooke et al., 2013; Barcos et al., 2016), and simulations (Willemse et al., 1996; Li et al., 2009; Strijker et al., 2013; Dasgupta et al., 2015; Nevitt, 2015, Frehner, 2016a, 2016b) investigated the behavior of transpression within contractional fault steps and the mechanical interaction between nearby fractures/faults. Mechanical modelling of a fault step avoids many of common assumptions, for example homogeneous deformation, inherent to kinematic models (Nevitt et al., 2014; Nevitt, 2015). These studies identified certain basic variables that influence the evolution of transpressional deformation in contractional fault steps, such as the fault overlap-to-separation ratio and the relative orientation of faults. The mechanical interaction between fault segments helps rationalize the overlap-to-separation ratio, their hook-shaped geometry (different from "hook fabric": Mukherjee and Koyi, 2010b), why some fractures/faults selectively terminate, whereas others propagate, and also deviates systematically from simple systematic slip distributions (Pollard and Aydin, 1988; Willemse et al., 1996; Lunn et al., 2008; Strijker et al., 2013; Lejri, 2015; Lejri et al., 2015). Static sliding friction coefficient strongly affects the fault mechanical properties and local stress field (Willemse and Pollard, 1998; Mutlu and Pollard, 2008; Maerten, 2010; Soliva et al., 2010; Ritz et al., 2015; Maerten et al., 2016; Mukherjee, 2017).

Numerical techniques, especially the finite-element (FE) method, are powerful to provide comprehensive insight beyond the direct observations, such as the stress state, strain and deformation patterns during and after the structural evolution. For example, Gölke et al. (1994) analyzed the vertical displacement, topographic variation, and pull-apart basin formation as a function of the relationship between fault geometries (underlap, neutral, and overlap states) in the releasing stepover along left-stepping left-lateral strike-slip faults using two-dimensional elastic FE-models. They showed two sub-basins separated by a broad zone of relative uplift forming in fault underlap. Bertoluzza and Perotti (1997) used a series of frictionless FE fault models to simulate the stress filed associated with pure strike-slip, transtensional, and transpressional conditions. They showed that the angle between the potential normal faults and the strike-slip faults strongly depended on the overall boundary conditions and only slightly on the rheological properties and the overlap-to-separation ratio of the faults. In addition, Misra et al. (2009) showed that reactivation of pre-existing fractures in presence of compressional shear loading conditions usually involved frictional sliding along the fracture wall which could produce local tensile stress concentrations that can cause the propagation of horsetail (Granier, 1985), splay (Martel, 1990), and tail or wing fractures (Willemse et al., 1997; Blenkinsop, 2000). Nevitt et al. (2014) and Nevitt (2015) studied a mechanical model of transpression within contractional planar overlapping faults in elastoplastic material using 2D plane-strain FE-modelling. In their model, the distribution of the minimum and maximum principal stretches deform locally in the step, so that no significant stretch (=final length/initial length) was deserved across the fault traces outside the step. As a result, the stretch ellipsoid varied in orientation throughout the step indicating

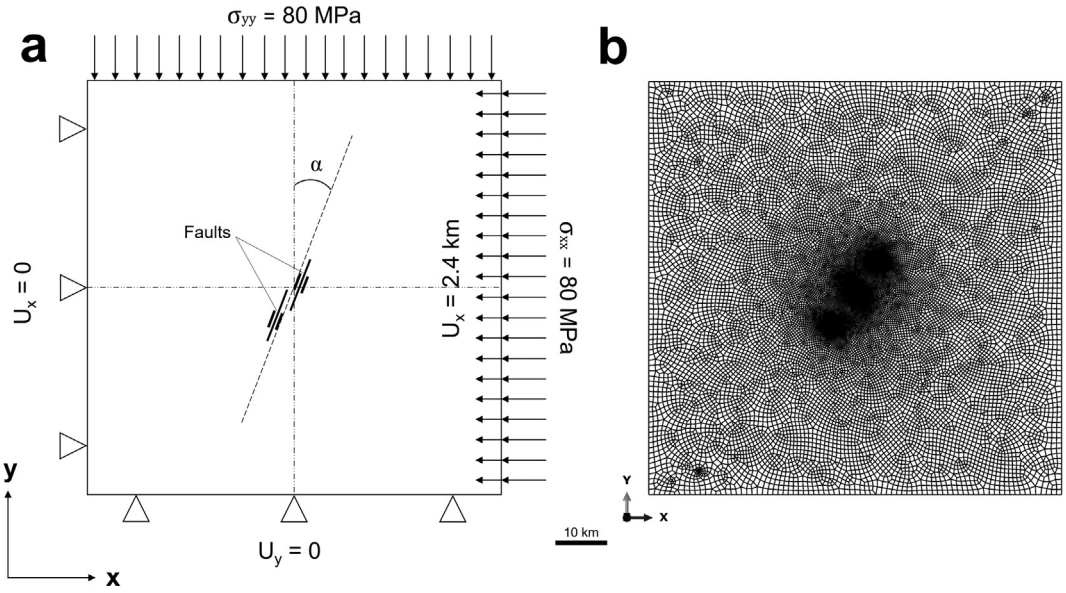

Fig. 2. a The general model set-up with two fault segments and boundary conditions. The finite element shown in (**b**) with decrease in size of element from the model edges towards the fault segments. The faults are pre-defined to strike at $\alpha = 0$, 30, 45, 60 and 90 in a clock-wise sense from the Y-axis, where α is the convergence angle.

heterogeneous deformation. However, the problem of stress distribution, strain localization, and transpression zone pattern in various convergence angles and geometries of frictional fault segments, parameters which strongly control the evolution of transpression zones within contractional fault step, has been less considered and compared with results of experimental modelling in these studies. Here the results of a systematic series of transpression zones are presented and compared with a range of natural, numerical, and experimental examples. It is of critical importance since deformation localizes around fault segment tips, the interaction between faults (as transpression boundaries) in different step geometries (such as underlap, neutral, and overlap configuration) is therefore expected to be significant. On the other words, knowledge of these problems using numerical and experimental models would be useful in interpreting transpression zones in areas of incomplete data.

We use a series of 2D FE-models through ABAQUS™ software package to simulate stress and strain features recorded in a transpression zone within the straight and parallel contractional fault step along a strike-slip fault system. We simulate the entire range of various tectonic regimes (i.e., pure strike-slip, transpression, pure contraction) by varying the convergence angles (0°, 30°, 45°, 60° and 90°) and analyze the stress/strain fields by applying different sets of boundary conditions. The purposes of this study are 1) to understand the role of strike-slip fault separation and amount of overlap on the development and evolution of transpression zones, 2) to predict the possible fault pattern inside the transpression zone, 3) stress distribution and strain localization patterns and validated and compared with analogue and numerical experiments performed by other authors, and 4) to simulate various fault step geometries in natural examples.

2. Finite element method

ABAQUS™ (ABAQUS/CAE), FE commercial program (ABAQUS™ tutorial version 6.14–2, 2014; www.simulia.com/) allows various element types and includes modules for several rheologies properties such as elasticity, plasticity (Mohr-Coulomb, Drucker-Prager, etc.), viscosity (linear, power law, etc.), and combinations thereof. Several types of boundary conditions (velocity, displacement, etc.), loadings (pressure, gravity, etc.), and contact formulations (surface to surface, general contact, node to surface, etc.) can be applied. Stress, strain, displacement and energy are among several output possibilities.

2.1. Model set-up

2D plain strain and linear elastic solid behavior (linear relation between stress and strain) is adopted for FE-modelling of transpression. The focus is on the interactions between two parallel, planar right-stepping left-lateral/sinistral strike-slip faults with equal lengths (a restraining step) that obey the Coulomb criterion for fault slip (Fig. 2a). Friction along the fault segments is constrained by a coefficient of 0.3–0.6 (Byerlee, 1978). In the present study it is 0.51 for sandstones (Pollard and Fletcher, 2005). Sliding occurs if traction on the fault exceeds 0.51 of the normal stress (Byerlee, 1978). The pair of fault segments strike obliquely to the direction of compressive normal stress applied to the model boundaries. The fault segments have a left-oblique component (Crider, 2001) that creates left-lateral movement/offset/slip. Surrounding the faults, we assume an isotropic homogenous linear elastic shell. Such an assumption was also made in similar studies by Goteti (2009), Strijker et al. (2013), Nevitt et al. (2014) and Nevitt (2015). Thus, the model presented in this work may not work for foliated rocks or for layered rock sequences. One reason for studying the elastic behavior is that the upper part of the lithosphere is often approximated as an elastic material (Turcotte and Schubert, 2014). Studies indicate that the rheology of the upper crust is elastic-plastic. Neverthless, because the rheology is approximate, we use the elastic models to only investigate spatial patterns and relative amplitudes of deformation. Our analysis is thus a linear approximation to a non-linear process. Therefore, we do not attempt to predict absolute uplift, subsidence, or slip along faults but only a relative pattern of deformation. The 2D FE-model considers plane strain, which is valid if the faults are much longer in the Z-direction than in the X- and Y-directions. The effects of topography and crust curvature are ignored. To avoid the effects of model boundary on stress distribution, the model dimensions are

Table 1
Modelling parameters (after Gölke et al., 1994; Pollard and Fletcher, 2005; Jaeger et al., 2007; Strijker et al., 2013).

Input parameters	
Elastic material properties	
Young's modulus (E)	22 GPa
Poisson's ratio (ν)	0.24
Fracture properties	
Friction coefficient (μ)	0.51
Applied compressive stress	
Normal stress (σ)	80 MPa

significantly larger (≥5 times) than the dimensions of the fault system (Misra et al., 2009), so that the applied boundary conditions simulate a far-field stress. A total of 23819 quad-dominant isotropic brick elements (23834 nodes) and two master left-lateral strike-slip faults describe a model of 80 × 80 km. Each fault segment is 10 km long. The size of elements decreases from the boundaries towards the faults to ensure sufficient accuracy whilst limiting computation time (Fig. 2b).

The used elastic parameters are as follows: Young's modulus (E) 22 GPa and Poisson's ratio (ν) 0.24 (based on Pollard and Fletcher, 2005; Jaeger et al., 2007) (Table 1). The elastic modelling parameters are kept constant for all experiments at physically realistic material property mean values representative for sandstones (Pollard and Fletcher, 2005; Jaeger et al., 2007). Previous numerical studies have shown that changing the elastic parameters does not produce significant changes in the modelling results (Gölke et al., 1994; Bertoluzza and Perotti, 1997; Bourne and Willemse, 2001). A compressive normal stress is applied to two adjacent boundaries of the model with a maximum value of 80 MPa based on Strijker et al. (2013). In addition, a displacement boundary condition is introduced on the right model boundary that produces a bulk shortening of 3% across the model. Lower and left boundaries of the model domain is constrained by the condition that $u_y = 0$ and $u_x = 0$, to prevent rigid body rotation and translation during loading (Nevitt et al., 2014; Nevitt, 2015) (Fig. 2a). These boundary conditions define shear planes both parallel to the fault steps and parallel to internal faults (Westaway, 1995), which obliquely connect fault steps.

2.2. Modelling strategy

We use a right-stepping configuration of two left-lateral faults to quantify the effect of different step geometries on the stress and strain distribution throughout the model. The faults are pre-defined to strike at α = 0, 30, 45, 60 and 90 in a clock-wise sense from the Y-axis, where α is the convergence angle (assuming that modelling was monitored through a top-view) (Fig. 2a). The main parameters investigated in the current model series are the convergence angle, the angle of offset between the master fault segments (Leever et al., 2011; Dooley and Schreurs, 2012), and the step geometries. In present study, transpression is considered in different overlap-to-separation situations such as underlap, neutral, and overlap. Growth of the pre-defined faults is not considered, instead the focus is on the resulting stress and strain distribution as indicators for the potential development of subsequent fractures/faults. Overlap (O) and underlap (U) are measured from fault tip to fault tip, parallel to the main fault strike. Separation (S) is measured orthogonal to the main fault strike (Dooley and McClay, 1997; Dooley et al., 1999; McClay and Bonora, 2001; Long and Imber, 2011; Dooley and Schreurs, 2012; Corti and Dooley, 2015). 'S' is 12.5% of the length of the fault segments (i.e. 1.25 km). Underlap and overlap are 25% of the length of the fault segments (i.e. 2.5 km). In addition, the step geometries are at 26° in case of underlapping step, 90° for neutral step, and 154° for the overlapping step (Fig. 3). These angles are measured between the strike of the main fault segments and the line jointing the tips of the faults in the step zone. All other parameters, including the separation between the master fault segments and the initial width of the offset area/weak zone (i.e. overlap and underlap size) are kept constant.

3. Results

With increasing obliquity, various displacements on the adjacent strike-slip fault segments and within the fault step result in a wrapped (non-linear) displacement pattern in the transpression zone but systematic paths (with a specific pattern and angle relative to the fault segments and far-field stress). The deformed geometry and stress and strain contours clearly show ~ strike-parallel contraction along the faults. Opposing slip along the fault segments within transpression zone warps and tilts the model transpression zone, resulting in a combination of simple and pure shear (i.e. general shear/sub-simple shear). The displacement vectors are 20–45° oblique to the regional applied shortening direction. Contraction localization along the transpression zone boundaries compared to no significant contraction/stretch immediately across the fault segments (the outer parts of the zone) and ensures that displacements remain oblique to the regional transport direction throughout the deformation. Within the transpression zone the interaction of stress fields near the tip of the faults produces a complex stress field. Outside the transpression zone, the maximum compressive stress (σ_1) orients sub-parallel to the applied regional compressive stress direction. Orientations of σ_3 (the minimum compressive stress) and σ_1 strongly depend on the structural position within the transpression zone. For underlapping fault steps, the highest rotation of these stresses is observed near the fault tips

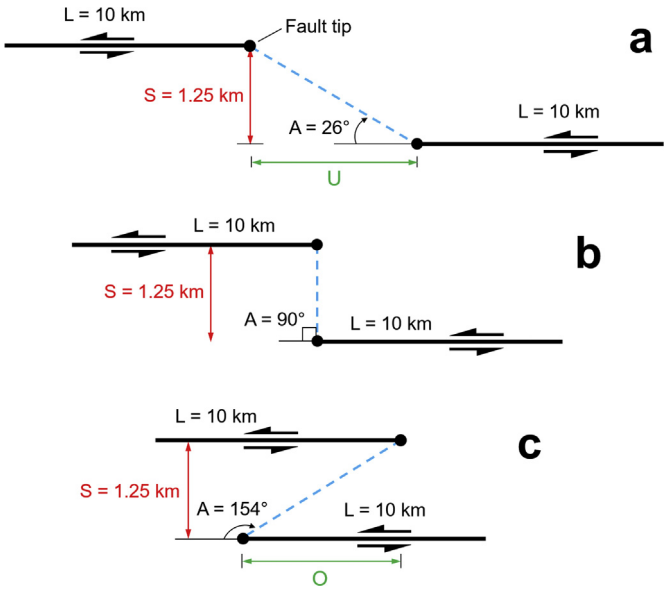

Fig. 3. Separation and angular relationships of the steps for the three models presented in this study (after Dooley and McClay, 1997; Dooley et al., 1999; Dooley and Schreurs, 2012; Corti and Dooley, 2015): 26°underlapping, 90° neutral and 154° overlapping steps. The angles of the steps are identical in numerical models. Separation (S) is 12.5% of the length of the fault segments. Overlap (O) and underlap (U) is 25% of the length of the fault segments. Underlap and overlap are measured from fault tip to fault tip, parallel to the master fault strike. Separation is measured orthogonal to the master fault trend.

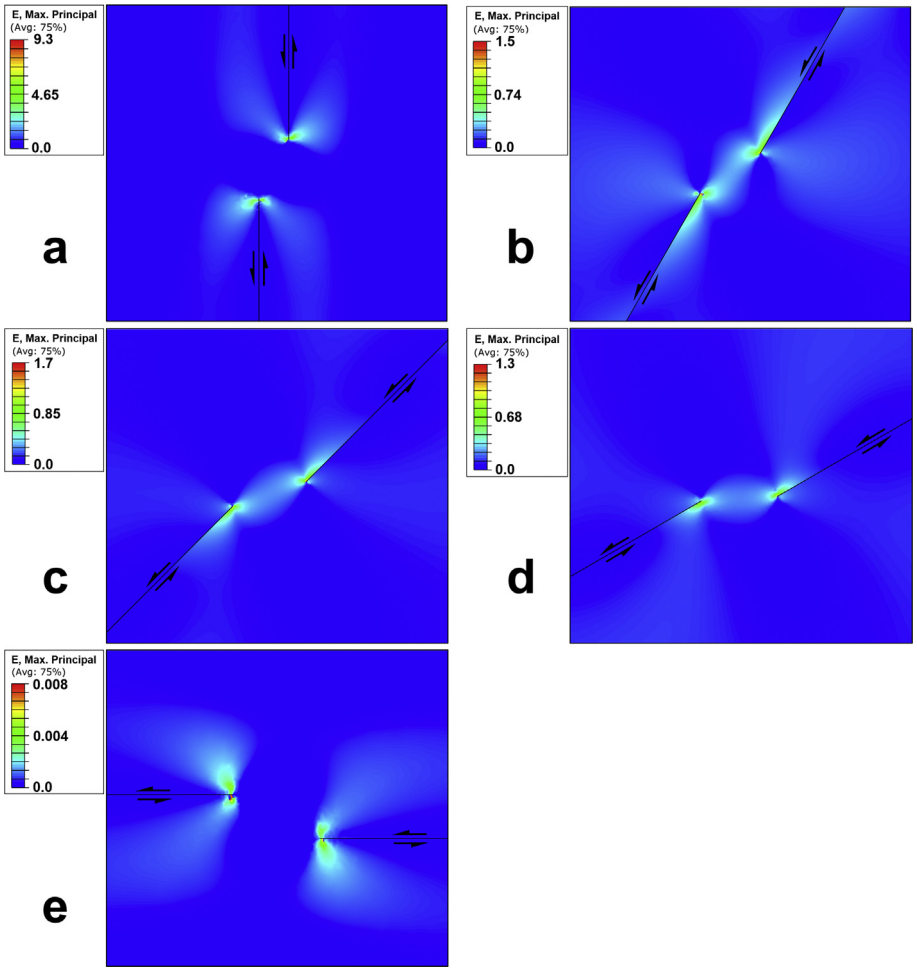

Fig. 4. Maximum principal strain distribution for underlapping steps under convergence angle of a) 0°; b) 30°; c) 45°; d) 60°; and e) 90°.

(20–70° relative to the fault segments), so that rotation decreases towards the central portion of the zone (almost parallel to the fault segments) (Fig. 4). For overlapping fault steps, σ_1 trajectories within the transpression zone are highly deflected, almost perpendicular to the applied stress orientation, which indicate a sigmoidal pattern (Fig. 5). σ_1 progressively rotates towards parallelism with the boundary faults as the convergence angle increases (from 30° to 60°). This sigmoidal pattern is created by two clockwise flow rotations around the fault tips due to friction effect and different shear component, from pure shear outside the fault steps towards simple shear along the fault segments. In a model with frictionless faults subjected to a remote shear stress parallel to the fault surfaces, the distribution of stress (Mises equivalent) and strain for contractional and extensional fault steps are mirror images of each other. Introducing friction and the contact properties necessary to prevent interpenetration impacts the two step geometries in distinct ways. This rotation of stress/strain vectors is higher than (10–20°) in the case of neutral fault steps (Fig. 6). The rotation of stress orientations from the regional transport direction increases with increasing overlap-to-separation ratio.

For neutral and overlapping fault step configurations, the compressional quadrants (the maximum principal stress) of the inner fault tips are located inside the transpression zone (Figs. 5 and 6). This condition results in a relatively high σ_3 in this part. Low-σ_3 zones develop in and near all fault tips and are located outside the fault segments (Fig. 7). In low-σ_3 zones (high stretch) wing cracks and horsetail arrays would therefore develop outwards along a curvilinear path, aligned with the local σ_1 trajectories (Fig. 8). A contractional linking damage zone, generally with shear fractures (mode II and III), multiple fault sets, and non-coaxial displacements (Segall and Pollard, 1980; Kim et al., 2000, 2001, 2004; Jones et al., 2004; Goteti, 2009; Goteti and Mitra, 2013, 2016; Choi et al., 2016) are created between the neutral and overlapping fault steps. Therefore that the strain magnitude reduce laterally from the central portion of the transpression zone towards the tips of the fault segments. σ_1 and the maximum principal strain trajectories show a sigmoidal shape and progressive rotation, implying a distributed simple and pure shear within the transpression zone (Fig. 8). The rhomboidal (for neutral steps) and sigmoidal (for overlapping steps) transpressional zones (or pop-up structure) may be bounded by listric, oblique-slip reverse faults. This distributed stress/strain trajectories cause block rotation.

Two main types of fault interaction occur (Aydin and Schultz, 1990; Gupta and Scholz, 1998, 2000; Fossen and Rotevatn, 2016): 1) “hard-linkage”: faults occurs where faults directly, or through a transfer/accommodation zone link together and 2) “soft-linkage”: faults interact when faults interact only through their stress fields and the associated strained zone is without crosscutting faults. Underlapping fault steps for $\alpha = 0–90°$, exhibit a well-developed σ_3 zone, roughly perpendicular to the fault segments that are linked together with a slightly oblique and a strong localization σ_3 zone within the transpression zone. The linkage zone of σ_1 trajectories

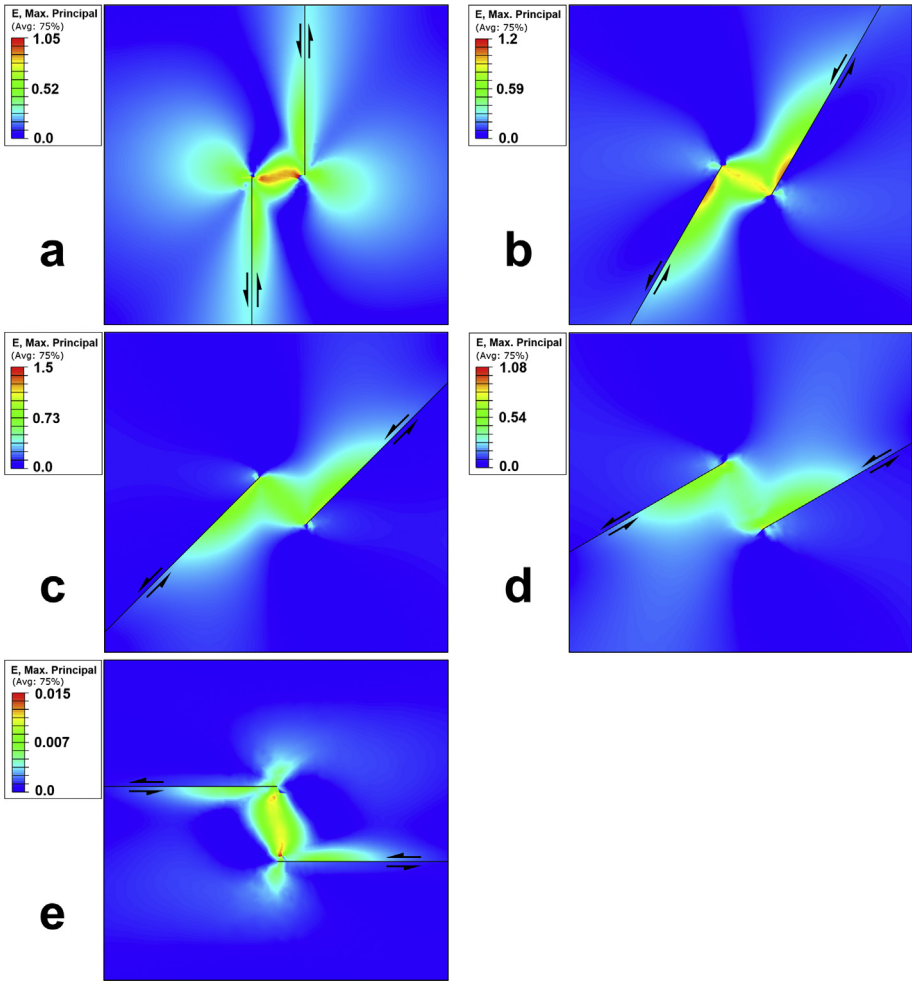

Fig. 5. Maximum principal strain distribution for neutral steps under convergence angle of a) 0°; b) 30°; c) 45°; d) 60°; and e) 90°.

does not develop for $\alpha = 0–90°$, where σ_3 zone localize in the tensional quadrant near the fault tips and σ_3 is actually relatively high in the central interaction zone of the fault segments. In all underlapping models, the lozenge-shape (Mukherjee, 2016) transpression zone are bounded by two dextral reverse faults. Differences between neutral and underlapping steps include higher stress concentration, increasing rotation, and the development of secondary shear displacement and structures in central portions of the zone due to the increasing amount of overlap. Stress concentration within transpression zones can exhibit uplift in 3-D models. In addition, overlapping steps display similar characteristics to the neutral steps, but develop a strong sigmoidal pop-up structure, bounded by curved, oblique slip reverse faults, and also increased rotation of stress trajectories in tips zone. These results resemble models of Dooley et al. (1999), McClay and Bonora (2001), and Dooley and Schreurs (2012).

In all present models, strain and stress trajectories rotation and variation in stress and strain magnitudes reflects a heterogeneous deformation, which ranges from approximately simple shear up to non-coaxial flattening strain. In other words, strain localization occurs in all models. In addition, the stretch ellipsoid (the amount of strain components after mapping all of them) varies in orientation across the step and constrain the heterogeneous deformation (e.g., Goteti, 2009; Goteti and Mitra, 2013, 2016). Increased friction along the faults tends to reduce the magnitude of the mean stress in the fault steps, as well as the size and extent of the region with the largest stress change (e.g., Kattenhorn and Pollard, 1999; Brankman and Aydin, 2004; Lejri, 2015; Lejri et al., 2015). The mean stress effectively shows uplift (contraction) and subsidence (extension) associated with faulting (Aydin and Schultz, 1990). In the overlapping fault steps with friction 0.51 and for all convergence angles, model results show low mean stresses to localize at fault tips and increasing mean stress towards the central portions of the zone as the two segments interact (Fig. 11). In neutral configurations, mean stresses localize more at fault tips than at the overlapping steps (Fig. 10). In contrast, for underlapping fault steps for all convergence angles, there is a concentrated low mean stresses between the segments (Fig. 9). The magnitudes of mean and shear stresses decrease and increase, respectively, from underlapping configuration toward overlapping fault steps, which is a consequence of the opposed relative motions of the two fault segments (Figs. 9–11) (e.g., Bürgmann and Pollard, 1992, 1994; Nemčok et al., 2002; Favreau and Wolf, 2009; Ritz, 2013; Ritz et al., 2015). Faults in brittle materials develop into the regions of lower mean stresses. Expectedly, results show that secondary faults develop away from one another (e.g. Segall and Pollard, 1980; Bürgmann and Pollard, 1994). Elastic models show that the mean stress, except for underlapping configurations, for all convergence angles is more compressive within the transpression zone than the region immediately outside the step and fault segment tips under tension. In all fault step models and convergence angles, except for $\alpha = 90°$, S_1 (the maximum stretch) trajectories make a high angles (45–90°)

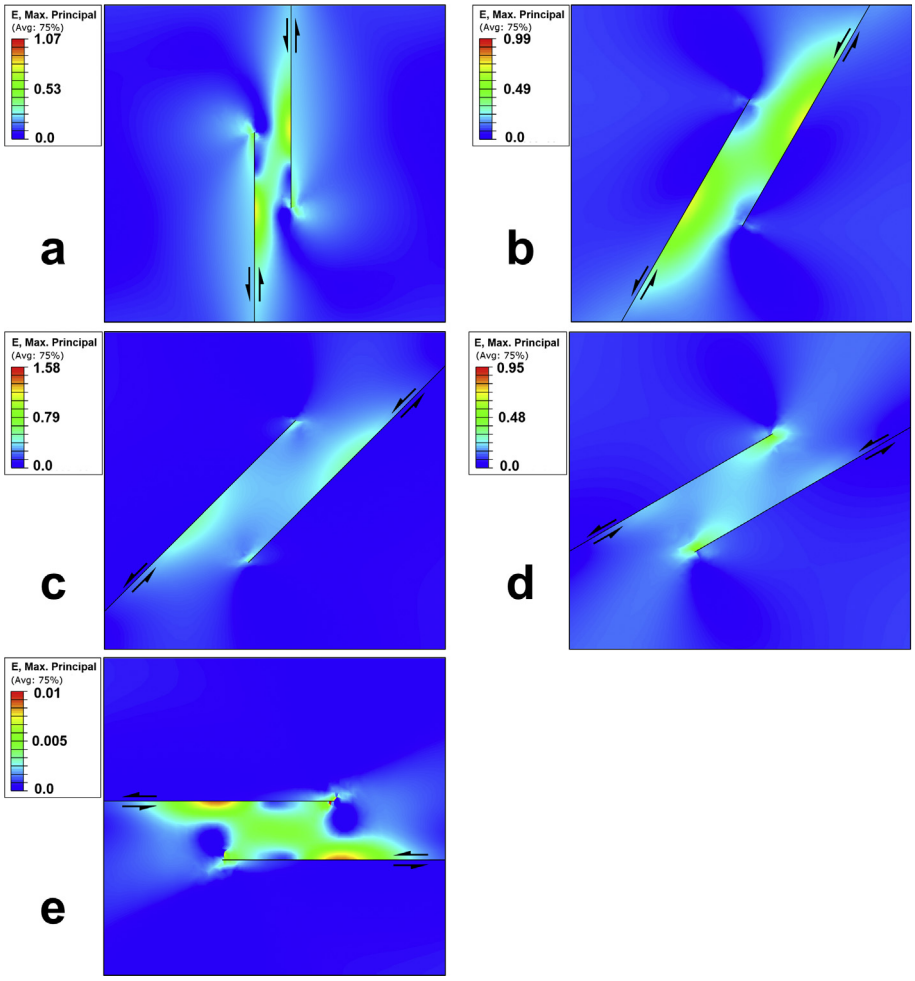

Fig. 6. Maximum principal strain distribution for overlapping steps under convergence angle of a) 0°; b) 30°; c) 45°; d) 60°; and e) 90°.

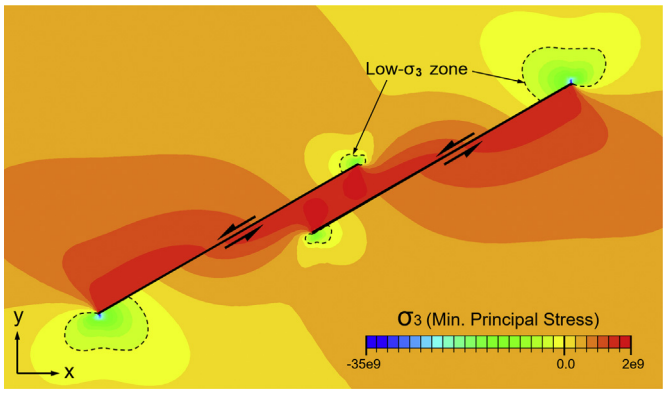

Fig. 7. σ_3 (the minimum compressive stress) distribution for overlapping steps under convergence angle of 60° with the minimum values at the fault tips. Low-σ_3 zones develop in the tensional quadrants outside the contractional fault step.

with the main fault segments. The angle between extensional structures, such as normal faults (parallel to the local σ_1 trajectories), and the main strike-slip fault segments (clockwise from the fault segment) in the ranges 65°–100°. The results suggest that even when the major faults are compressed orthogonally and the overall deformation is plane strain, transpression zones can be involved by a complex three dimensional stress/strain field inconsistent with the regional strain field.

The Von Mises equivalent stress, which is a function of the principal stress difference and the maximum shear stress, in the transpression zone evolves into a stress field that differs from the far-field stresses outside the zone. This modification of stress field is more prominent in the case of overlapping steps than the neutral and underlapping steps. In almost all configurations, lobes of enhanced Von Mises equivalent stress extend beyond the fault tips and slightly beyond the fault segments (Figs. 12–14). In general, neutral and underlapping fault steps result in higher distortional stresses/strains at fault tips and in the central contractional area than in the case of overlapping faults, characterized by higher Von Mises stress in the transpression zone. This is because, distortion of the contractional zone accommodates most of the extension. Depending on the proximity between the faults, these high stresses can promote fault growth along strike if the initial spacing between the fault segments is large or can promote the formation of secondary oblique structures linking the main fault segments if the faults are close-spaced (e.g., Segall and Pollard, 1980; Bürgmann and Pollard, 1992, 1994; Nevitt et al., 2014; Nevitt, 2015).

Figs. 15 and 16 present data collected along two transects through the overlapping fault step models for convergence angles 30 (Figs. 15a,b and 16a,b), 45 (Figs. 15c,d and 16c,d) and 60° (Figs. 15e,f and 16e,f). Transect 1 parallels faults through the center of the transpression zone while transect 2 orient perpendicular to the fault segments. The two transects record very different profiles

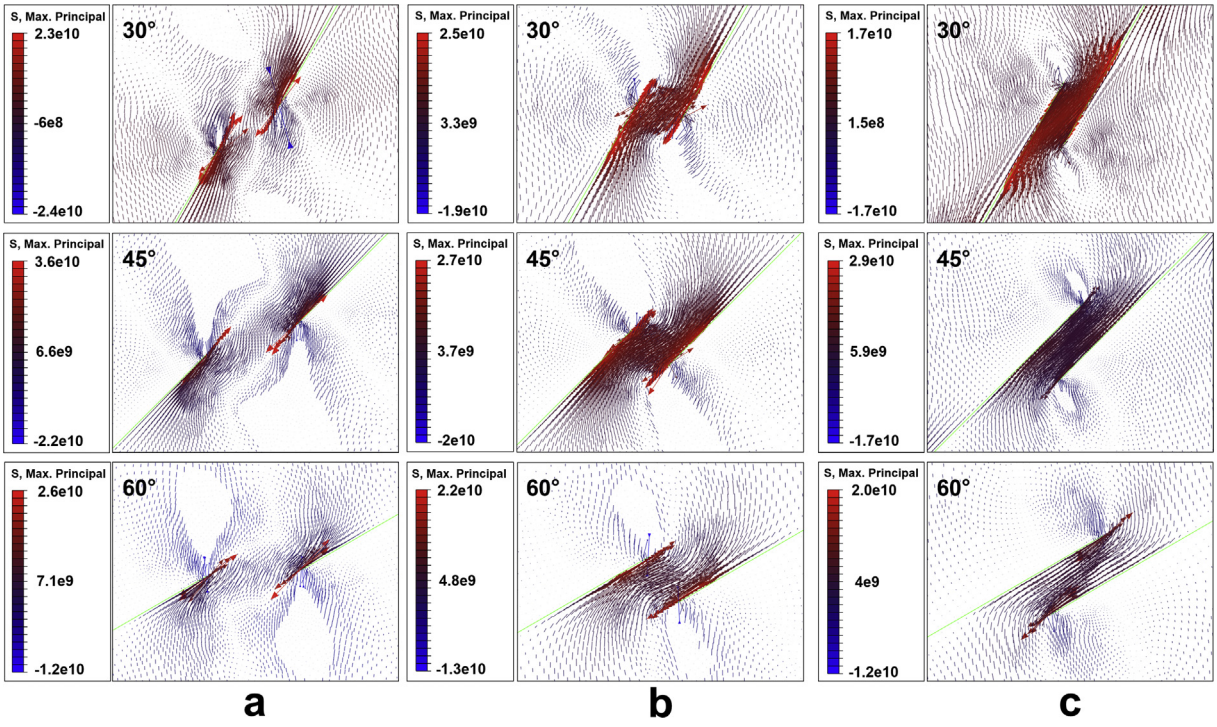

Fig. 8. Orientation of σ_1 for transpression zones within contractional fault step configurations with different combinations of overlap-to-separation ratio. **a** Underlapping steps; **b** Neutral steps; **c** Overlapping steps.

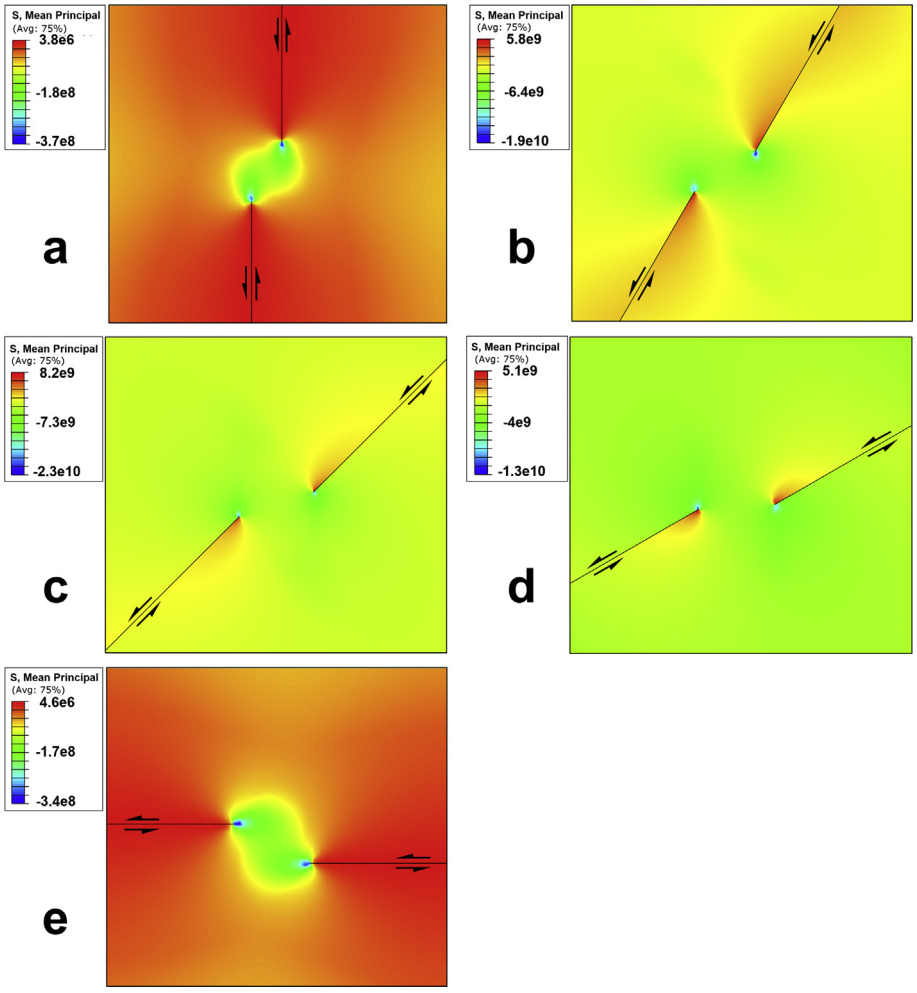

Fig. 9. Mean principal stress distribution for underlapping steps under convergence angle of a) 0°; b) 30°; c) 45°; d) 60°; and e) 90°.

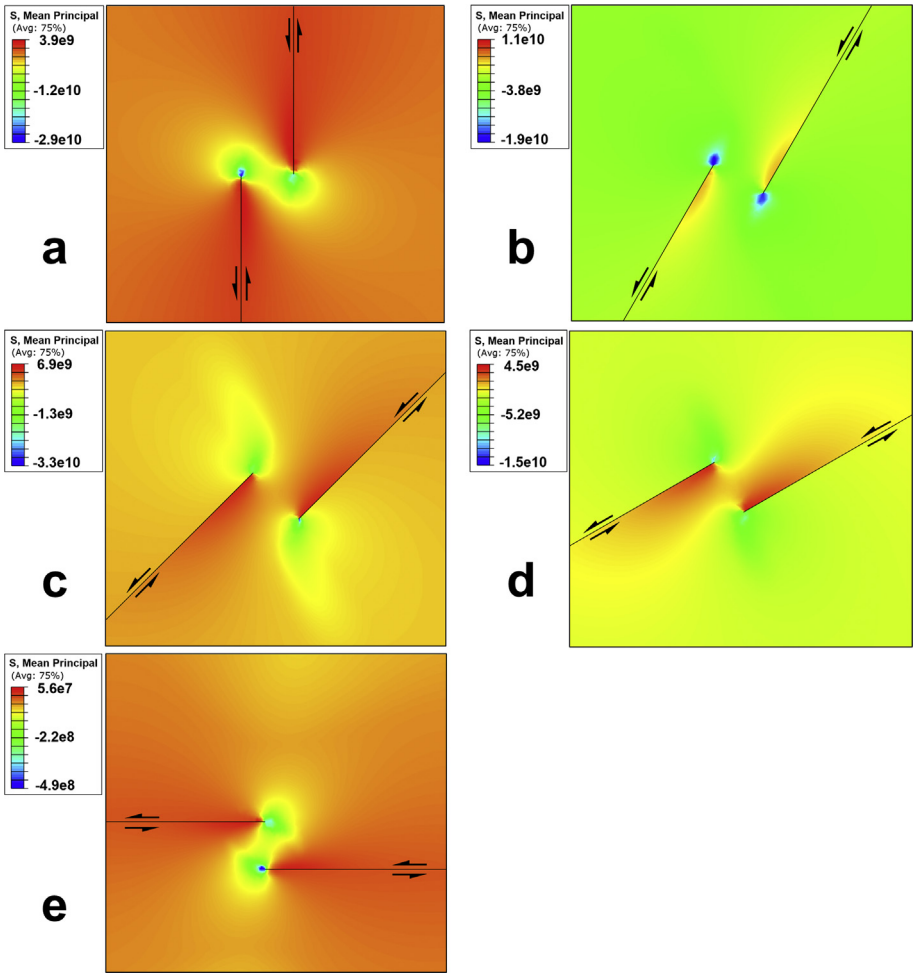

Fig. 10. Mean principal stress distribution for neutral steps under convergence angle of a) 0°; b) 30°; c) 45°; d) 60°; and e) 90°.

of the principal stretch (S_1) and shear stress (S_{12}) magnitudes. Transect 2 demonstrates that in the direction orthogonal to the step-bounding faults, the stretch is focused into the step region, so that stretch difference increases with increasing convergence angle. On the other hand, transect 1 show that deformation decreases more gradually in the direction parallel to the faults.

4. Discussion

At the transpression zone, in addition to local uplift, contractional structures such as folds, thrust faults and pressure solution seams form on the contractional quadrant of the fault termination and often parallels the local σ_3 axis, in general. At the tips of mode II cracks or strike-slip faults, the local perturbation of the main stress field causes splay faults to occupy three distinct domains dominated respectively by shear, contractional, and extensional structures (Maerten et al., 2002, 2006; Goteti, 2009; Goteti and Mitra, 2013, 2016; Upton and Craw, 2016). Altering the strike of the fault segments relative to the direction of applied compressive stress (i.e., convergence angle) alters the geometry of linkage, because the symmetry of the system change. Oblique slip and convergence angles affect both the magnitude and the shape of the regions of stress concentration around the fault segments and within the transpression zone, showing changes in $\alpha = 30–60°$ in comparison to $30° > \alpha$ and $60° < \alpha$. According to the maximum principle strain trajectories, before forming rhomboidal and sigmoidal transpression zones, secondary faults develop parallel to the fault segment displacement, but later parallel to the contractional step and accommodate an oblique-slip. The sigmoidal shape of the transpression zone in overlapping steps is due to increases in the amount of overlap, which results in a wider transpression zone and well-developed crosscutting faulting or internal faults (Westaway, 1995) linking the fault segments. These crosscutting faults are P-shear splay faults (see Misra and Mukherjee, in press-2 for field examples) or linkage that accommodates fault parallel shortening as shearing proceeds, and are outnumber R-shears (Keller et al., 1997; Schreurs and Colletta, 2002; Barreca and Maesano, 2012; Pennacchioni and Mancktelow, 2013). Furthermore, antithetic faults can develop in an en-échelon array (in the high angle ~70°–90° in neutral and underlapping steps and ~30–45° for overlapping steps) along the high mean stress zones in between the fault segments (e.g. Kim et al., 2004; Barreca and Maesano, 2012; Pennacchioni and Mancktelow, 2013). Since 2D models presume faults to be vertical, this mean stress perturbation between fault segments is less in three-dimensional models. This is because the depth of faults is relatively short with respect to the model dimensions. More concentrated compressive stress on both sides of rhomboidal and the sigmoidal transpression zone can define a transpression zone with greater uplift in central areas (e.g. Upton et al., 2009) and make a doubly plunging anticlinal structure. These restricted sigmoidal zones to contractional fault steps appear like S-C ductile fabrics, mineral fishes, recrystallization and crystal-

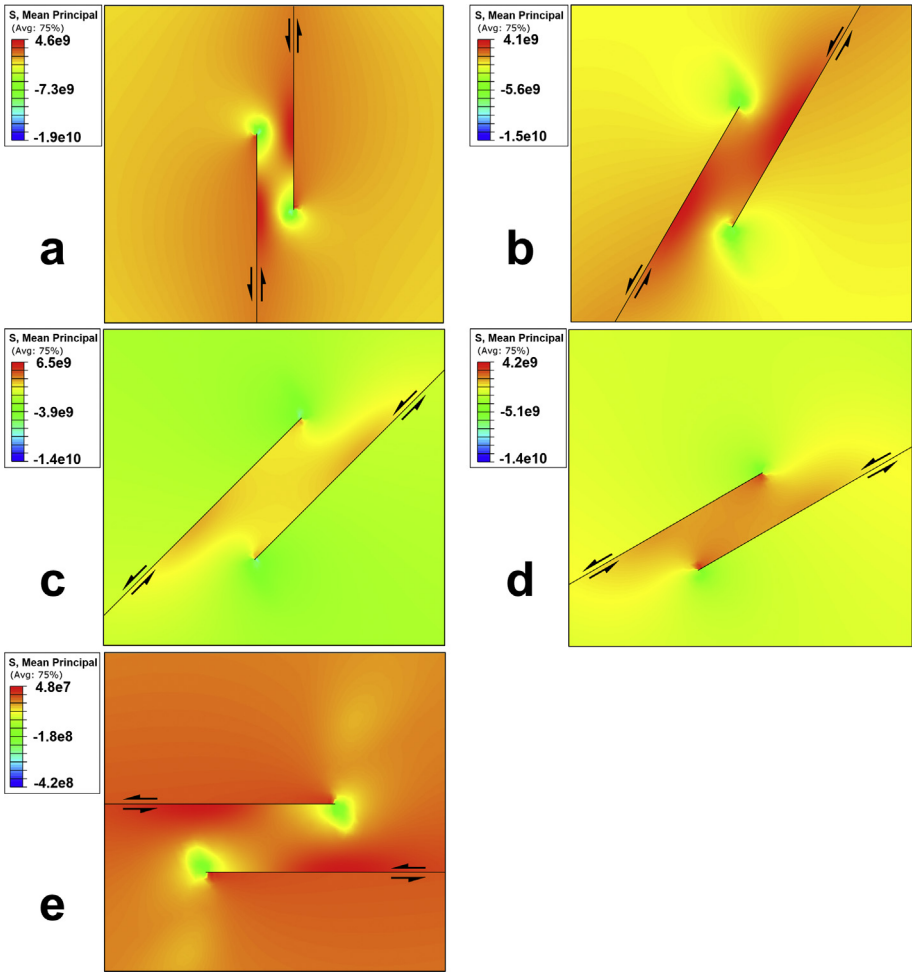

Fig. 11. Mean principal stress distribution for overlapping steps under convergence angle of a) 0°; b) 30°; c) 45°; d) 60°; and e) 90°.

plastic flow with a component of non-coaxial flow on the macroscopic-to microscopic-scales (Lister and Snoke, 1984; Passchier and Trouw, 2005; Mukherjee, 2010b, 2011; Fossen, 2016). Under contractional condition in the fault steps, wing cracks and horsetail arrays development is restricted to $30^\circ \leq \alpha \leq 60^\circ$ (intermediate values of α), whereas S_1 trajectories concentrate at the fault segment tips.

Fault interactions can give rise to a broad variety of local structures that can be explained in terms of the variations in the strain field predicted by the model. These results are consistent with recent field studies that point towards a complex deformation pattern in transpression zones within contractional fault steps. As the results show, three-dimensional stress/strain in the transpression zone with overstepping strike-slip systems typically involve rotation around a vertical axis. Rotational processes can be the attitude of this axis in natural prototype (such as thrust emplacement, local develop of oblique-slip faulting, and exhumed strike-slip systems) (e.g. Garfunkel and Ron, 1985; Channell et al., 1990; Oldow et al., 1990; Renda et al., 2000; Monaco and De Guidi, 2006; Avellone et al., 2010; Upton and Craw, 2014; Cao and Neubauer, 2016; Nabavi et al., 2016c). Stress/strain trajectories from underlapping steps to overlapping configuration reveal that transpression within contractional fault steps locally accommodate the regional stress field and may not be locked. Simultaneous simple shearing and pure shearing within transpression zone change the fault type and orientation when the boundary fault changes from pure strike-slip to oblique reverse-slip within the zone and generate an asymmetrical section across the zone, which symmetric geometries are only found in its central parts (e.g., Dooley et al., 1999; McClay and Bonora, 2001). Rotation of fault planes have already been simulated in models and ascertained in nature (review in Mukherjee, 2014a,b).

Various field studies on outcrop to regional scale transpression structures clearly reveal spatial and temporal variations in the extension directions with increasing contraction on the major faults. The broad variety in the orientations and kinematics of these local structures cannot be directly correlated to the deformation on the major faults and vice-versa. The maximum finite strains rotate towards the regional transport direction and transpression zone boundaries with progressive deformation. Therefore, local structures oblique to the major faults are common in incipient transpression zones. In subsequent stages of deformation, with increasing contraction on the faults, these local structures may be overprinted by younger generations of less oblique structures or, may be reactivate in conformance with the strain field (e.g., Ismat and Mitra, 2001). Numerical results suggest that even for an isotropic material, fault interactions result in non-coaxial strain paths and complex stress fields within transpression zones. The non-coaxiality of deformation in transpression zones (Nabavi et al., 2016b) has important implications for interpreting attendant structures and strain partitioning. Kinematics of oblique convergence and various related structures need to be cautiously

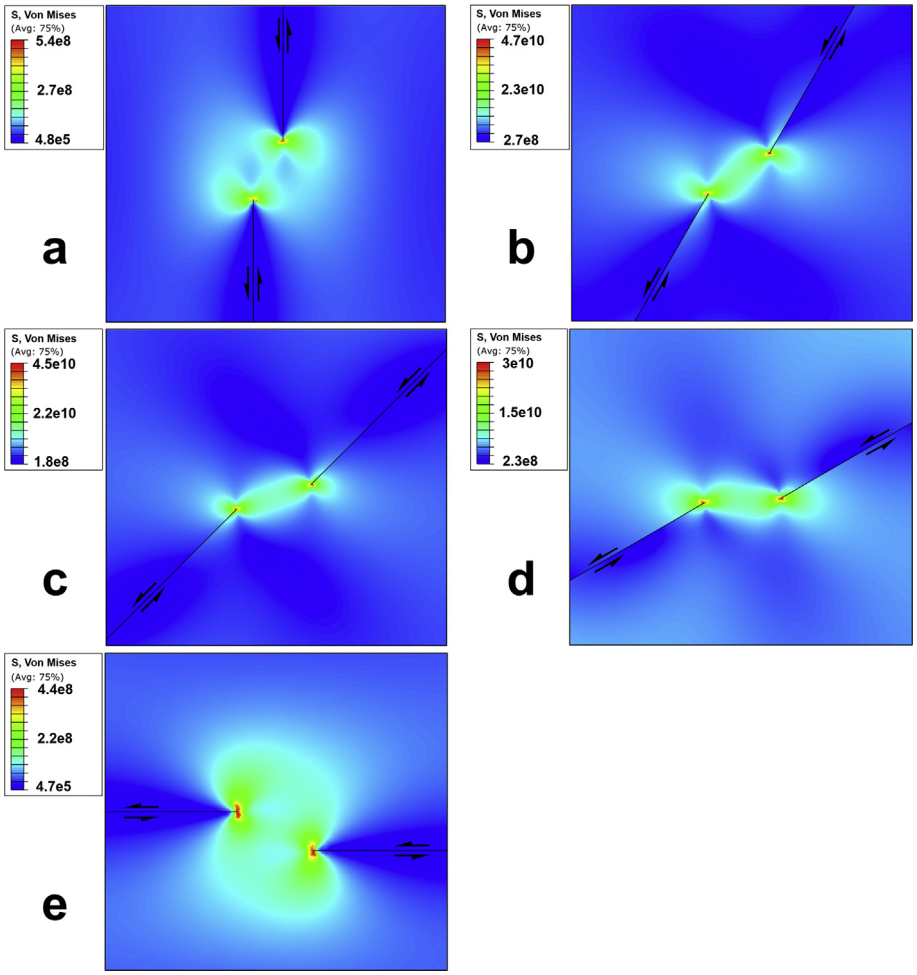

Fig. 12. Von Mises equivalent stress distribution for underlapping steps under convergence angle of a) 0°; b) 30°; c) 45°; d) 60°; and e) 90°.

interpreted in terms of the 3D strain field, noting that the strains/stresses vary both temporally and spatially in the transpression zone. In fact, field studies in contractional settings, such as Zagros fold-and-thrust system (Sarkarinejad, 2007; Sarkarinejad and Azizi, 2008; Sarkarinejad et al., 2010, 2013) and Alborz Mountain Range (Ballato et al., 2013; Nabavi et al., 2016b, 2016c), clearly demonstrate that non-coaxial flow in rocks (Mukherjee et al., 2012; Mukherjee, 2013b) can result in a wide range of finite strain ellipsoid orientations corresponding to a single overall compressive stress regime. Note that the imposed maximum regional compressive stress in the present study is 80 MPa. In transpression zones characterized by higher convergence and contraction on the major fault steps, the non-coaxiality of the deformation will conceivably be significantly higher. Lithological and mechanical heterogeneities in natural transpression zone rocks further complicate the relationship between strains and stress.

4.1. Modelling the Esmail-abad – West Neh contractional fault step (Sistan Structural Zone, southeastern Iran)

4.1.1. Sistan Structural Zone

The Sistan Structural Zone (SSZ) in southeastern Iran a ~N trending Cretaceous-Tertiary orogenic belt more than 700 km along the border area between Central Iran and Helmand (Afghan) blocks (Fig. 17a and b) (Tirrul et al., 1983; Walker and Jackson, 2004; Mohammadi et al., 2016). After the Afghan block rifted from the Lut block in Early Cretaceous, the SSZ formed by closing the north-south extension of the Neotethys Ocean (called the Sistan Ocean) between the Central Iranian Lut continental block and the Afghan microcontinent during Campanian to Paleocene times along an eastward dipping subduction zone (Camp and Griffis, 1982; Tirrul et al., 1983; Agard et al., 2011; Bröcker et al., 2013; Bayet-Goll et al., 2016; Mohammadi et al., 2016). The SSZ comprises three main sub-zones (Camp and Griffis, 1982; Tirrul et al., 1983; Perelló et al., 2008; Fotoohi-Rad et al., 2009; Saccani et al., 2010; Angiboust et al., 2013; Mohammadi et al., 2016) (Fig. 17b): 1) the Rutak Complex (the oldest part of SSZ) to the East, which consists of Cretaceous flysch, high-pressure, low-temperature metabasites, fault-bounded masses up to 15 km long ophiolitic units, and a metamorphic mélange; 2) the Neh Complex as accretionary wedge to the West, which consists of late Cretaceous to Eocene flysch and some ophiolitic units; and 3) the Sefidabeh Basin, which overlies the Rutak and Neh Complexes unconformably and consists of unmetamorphosed fore-arc sediments of Maastrichtian to Eocene age. The SSZ contains various backthrust and active sub-parallel strike-slip faults as en-échelon arrays that formed many extensional (releasing) and contractional (restraining) steps/bends along the faults. Generally, the deformation in eastern Iran is controlled by the right-lateral strike-slip that is north-south to northwest-southeast trending (Berberian et al., 2000; Walker and Jackson, 2004; Parsons et al., 2006; Mohammadi et al., 2016).

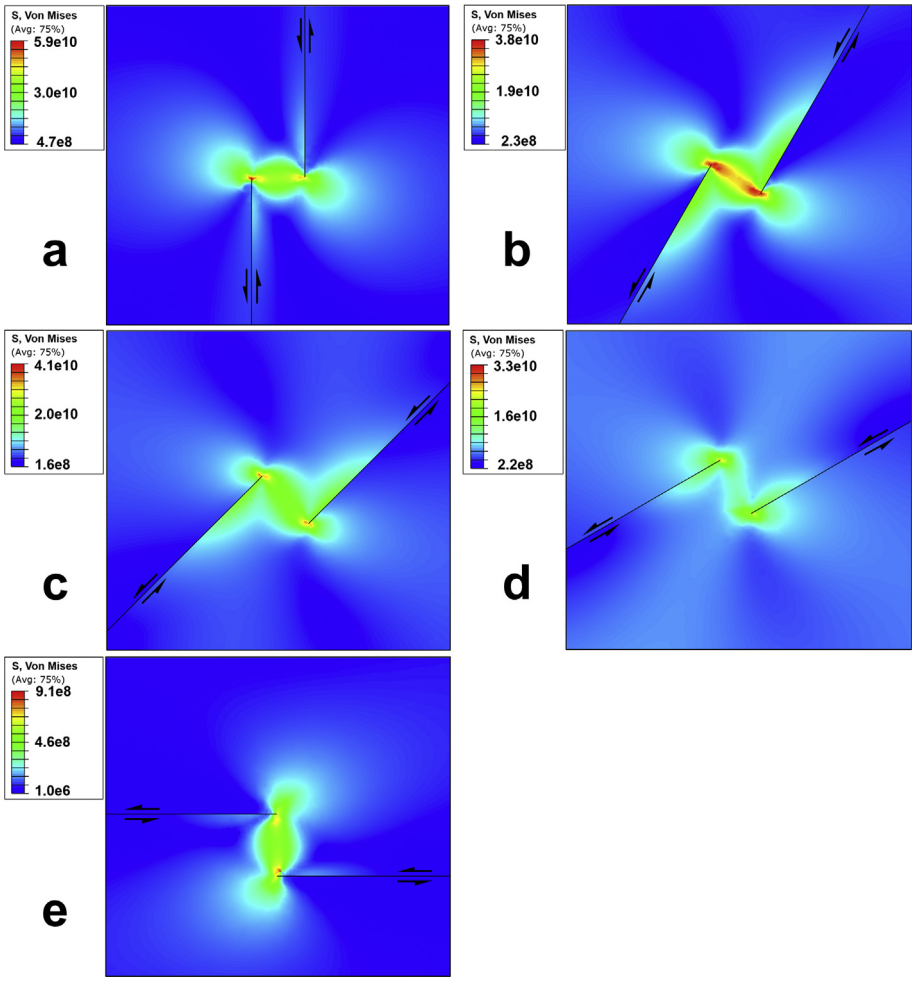

Fig. 13. Von Mises equivalent stress distribution for neutral steps under convergence angle of a) 0°; b) 30°; c) 45°; d) 60°; and e) 90°.

4.1.2. Esmail-abad – West Neh contractional fault step

The Esmail-abad right-lateral strike-slip fault with a reverse-slip component is one of the segments of the Nehbandan continental basement fault, which is the structural boundary between the SSZ and the Lut block structural zones (Fig. 17c and d). It extends as ~ N trending ~70 km long fault between the Sah-abad and Nehbandan areas (Walker and Khatib, 2006). The West Neh fault is one of the right-lateral strike-slip segments of the Neh fault system and also trends N. These two fault segments form a left-stepping geometry and create a contractional step (Fig. 17c and d). According to the Iranian Permanent Global Positioning System Network (IPGN) (www.ipgn.ncc.org.ir) the velocity of eastern Iran is 8 mm/yr and the local compressive stress directs N26°E. Hence, a transpressional zone, named of Kuh-e-Hori, between the two fault segments has formed at an altitude of ~2700 m (Fig. 17c–e). At the surface, this transpression zone comprises shale, sandstone, and limestone lenses (partly metamorphosed) (Paleogene) with ultrabasic, volcanic rocks (Neogene). Quaternary terraces and alluvial fans are outside this zone. The Kuh-e-Hori transpression zone has a central rhomboidal shape, is bounded by two outer steep reverse faults, and its maximum uplift is located in the center of the fault step. Given the far-field compressive stress direction of N26°E and the transpression zone characteristics, the fault segments indicate a neutral step geometry (i.e., 90° restraining step). The structural features of Kuh-e-Hori correlates well with our FE-results in the neutral step geometry at far-field compressive stress direction of N30°E (Fig. 18a–d). The circular pattern of the maximum principal stress trajectories, deduced by means of McClay and Bonora (2001) and Dooley and Schreurs (2012), is located much more around the fault tips than within the transpression zone, which is dominated with highlands (i.e., Kuh-e-Hori). Also, the maximum principal strain trajectories concentrate within the transpression zone along a NW-SE direction that developed contractional structures such as folds and reverse faults. The results show the capability of fault segments in the transpressional zone to increase the mean principal stress during all simulated stages of the transpression zone. The mean stress pattern can be characterized as having greater magnitude within transpression zone than at the fault tips and outside the zone (as Sahl-abad subsidence) (Figs. 17c and 18c). The maximum stress concentration in the central part of the zone shows the relative motions of the advancing sides of the two fault segments, which are opposed in the zone and control the mean stress concentration (Fig. 18b). Six topographic sections across the Kuh-e-Hori (AA′–FF′) (Fig. 17d and e) shows a moderate, yet distinct asymmetry and maximum uplift in the central part of the zone (as per Dooley et al., 1999; McClay and Bonora, 2001; Dooley and Schreurs, 2012 analogue models). The asymmetrical uplift in response to obliquely applied stress loading is controlled by the finite fault length. The asymmetric transpression zone is bounded by moderately dipping, and oblique reverse faults. Asymmetric geometries decrease in the central parts. In addition, serial sections (from AA′-EE′) (Fig. 17e) show that the Kuh-e-Hori transpression

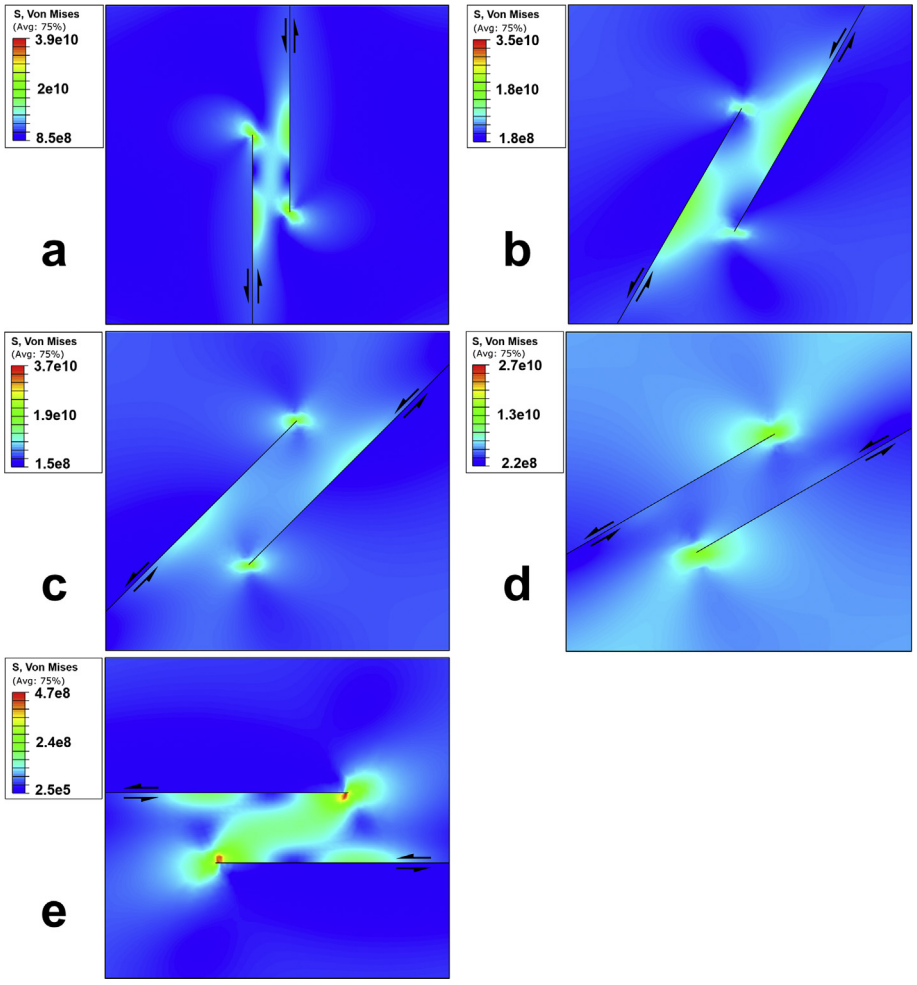

Fig. 14. Von Mises equivalent stress distribution for overlapping steps under convergence angle of a) 0°; b) 30°; c) 45°; d) 60°; and e) 90°.

zone is formed as a doubly plunging anticline.

5. Conclusions

Stress distribution and strain localization patterns were obtained for a set of 2D FE-models of a transpression zone related to two pre-existing right-stepping left-lateral strike-slip fault segments as a function of the remotely applied compressive stress. Linear elastic rheology and plain strain conditions were assumed. In each simulation, different convergence angles α, 0 (pure strike-slip), 30, 45, 60 and 90° (pure contraction) were applied to the three representative end-member fault segment interaction models, which were underlapping, neutral, and overlapping contractional steps. The numerical results indicate that the displacement vectors are oblique to the regional transport direction throughout the deformation history. With increasing contraction, the magnitude of displacement within the transpression zone increases. Orientations of the σ_1 and σ_3 orientations strongly depends on the structural position within the transpression zone. In low-σ_3 (the minimum compressive stress) zones, which are concentrated around fault tips, wing cracks and horsetail arrays would therefore develop outwards along a curvilinear path. For overlapping fault steps, the σ_1 (the maximum compressive stress) orientations within the transpression zone are highly deflected and rotate to become parallel with the zone bounding strike-slip faults. This pattern was created by two clockwise flow rotations around the fault tips due to friction effect and different shear components, from pure shear outside of the fault steps toward simple shear along the fault segments. This causes the perturbed stress field which reflects the heterogeneous nature of deformation. Lozenge-shaped transpression zones are characterize the underlapping steps, whereas rhomboidal and strongly sigmoidal transpression zones are characteristics of neutral and overlapping steps, respectively. Transpression zones are affected by curved, synthetic and antithetic oblique-slip reverse faults that cause block rotation between segments and show the asymmetric geometries in the section. Symmetric geometries are only found in the central parts of the zone. Within overlapping fault steps, crosscutting faults transect the central parts of the transpression zone as hard-linkage and the clear contractional linking damage zone. The mean stress pattern is similar to the pattern in contractional steps and decreases and increases, respectively, from underlapping configuration toward overlapping fault steps. Two pairs of local minimum (at the extensional quadrant of the tips) and maximum (at the compressional quadrant of the tips) mean stress patterns developed at the tips of the fault segments. In general, mechanical interaction between the fault segments decreases with increasing the overlap-to-separation ratio. Oblique slip and convergence angles affect both the magnitude and the shape of the regions of stress concentration around fault segments and within the transpression zone, so that models show the changes in $\alpha = 30–60°$ compared with $30° > \alpha$ and $60° < \alpha$. The natural example of the Kuh-e-Hori

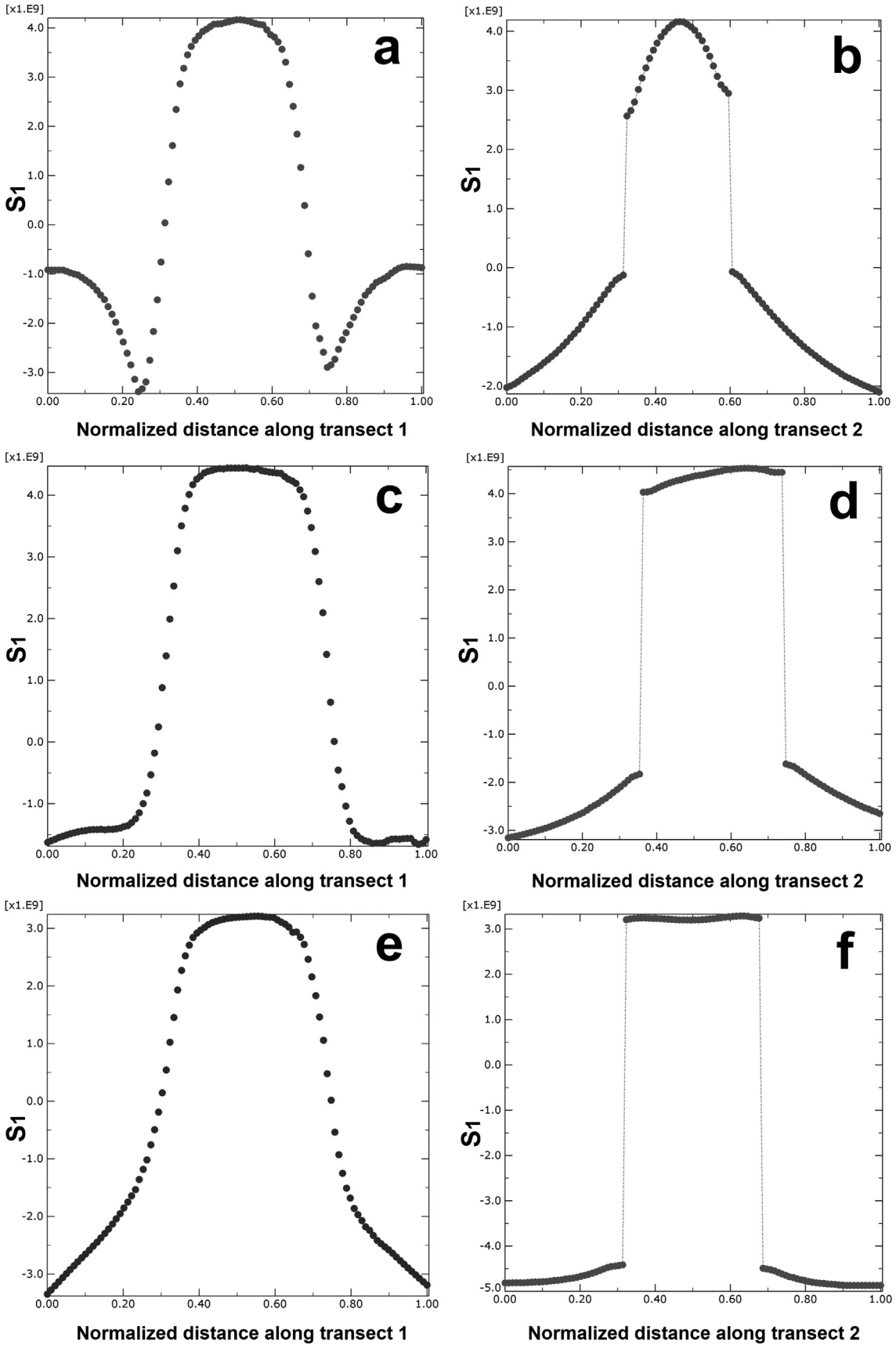

Fig. 15. Model results of maximum principal stretch (S_1) for overlapping steps in convergence angles 30° (**a,b**), 45° (**c,d**) and 60° (**e,f**). Left and right columns show transect 1 and transect 2, respectively.

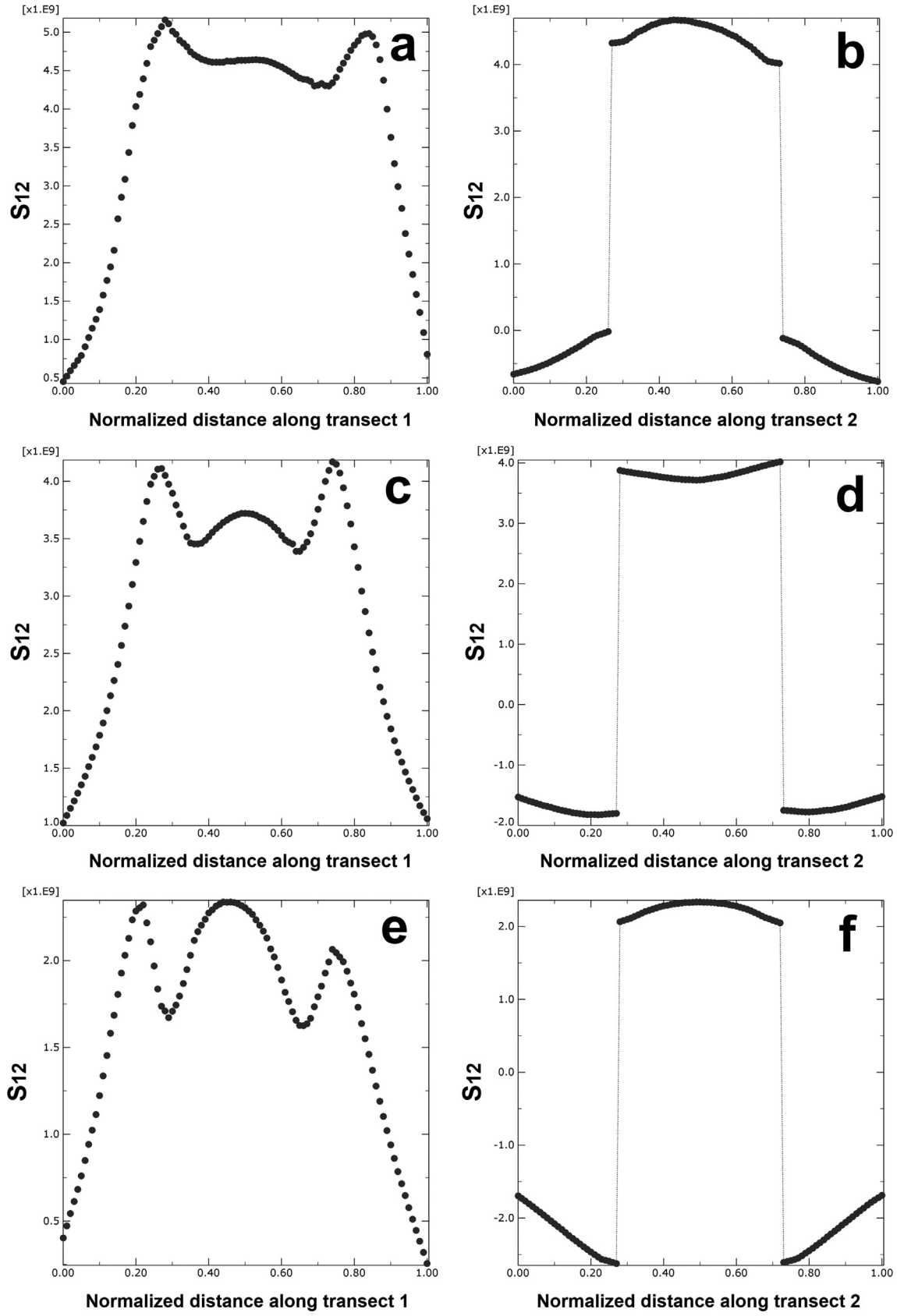

Fig. 16. Model results of shear stress (S_{12}) for overlapping steps in convergence angles 30° (**a,b**), 45° (**c,d**) and 60° (**e,f**). Left and right columns show transect 1 and transect 2, respectively.

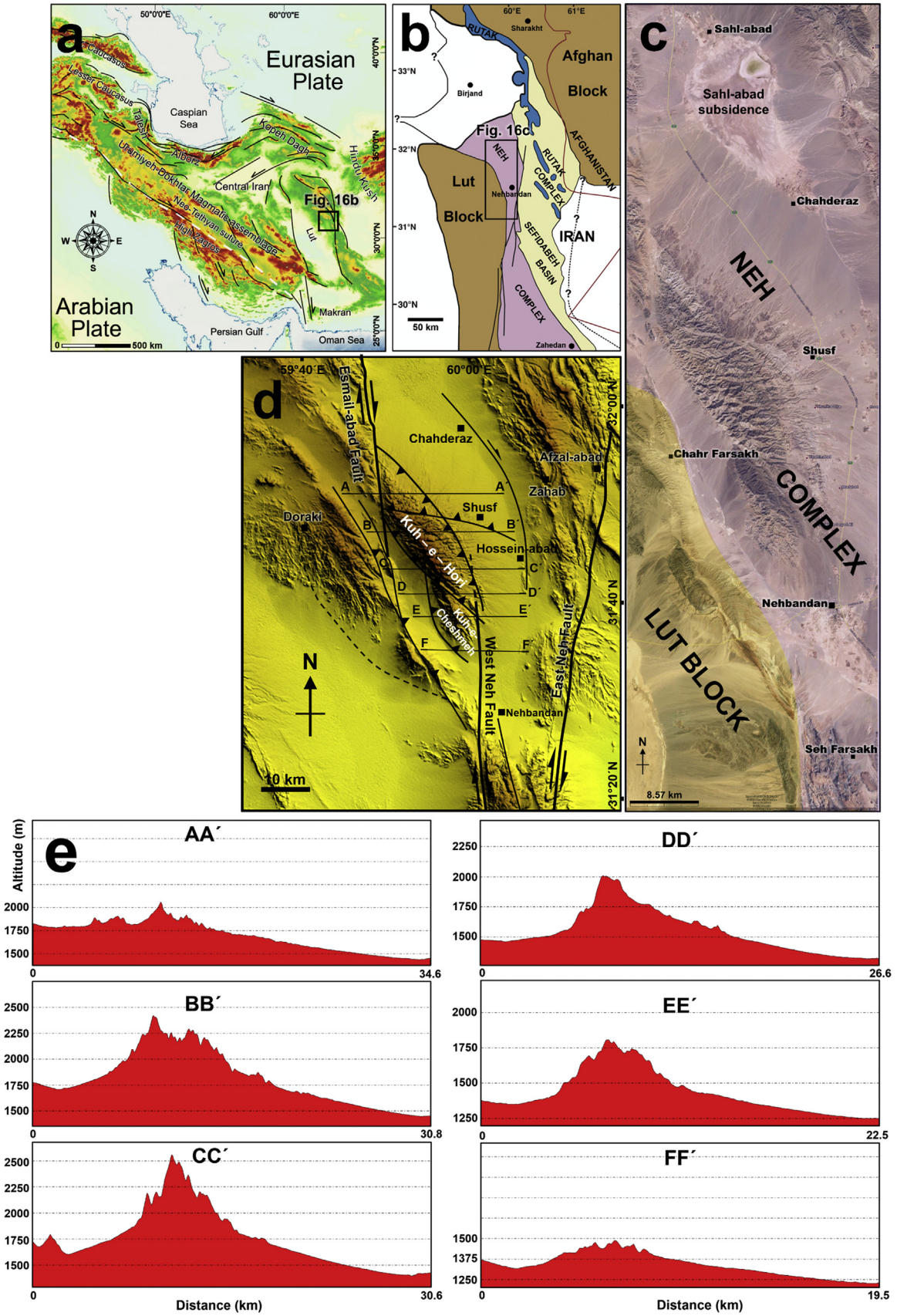

Fig. 17. **a** Regional overview of Iran; **b** Simplified geological map of the northern part of the Sistan Suture Zone (after Fotoohi-Rad et al., 2009; Bröcker et al., 2013; Bayet-Goll et al., 2016). **c** Google Earth™ image of the Kuh-e-Hori transpression zone from the map view. **d** Digital elevation model with simplified structural map of the Kuh-e-Hori transpression zone between the Esmail-abad and West Neh left-stepping right-lateral strike-slip fault segments. **e** Serial topographic sections across the Kuh-e-Hori transpression zone. Sections are named in accordance with (Fig. 16d).

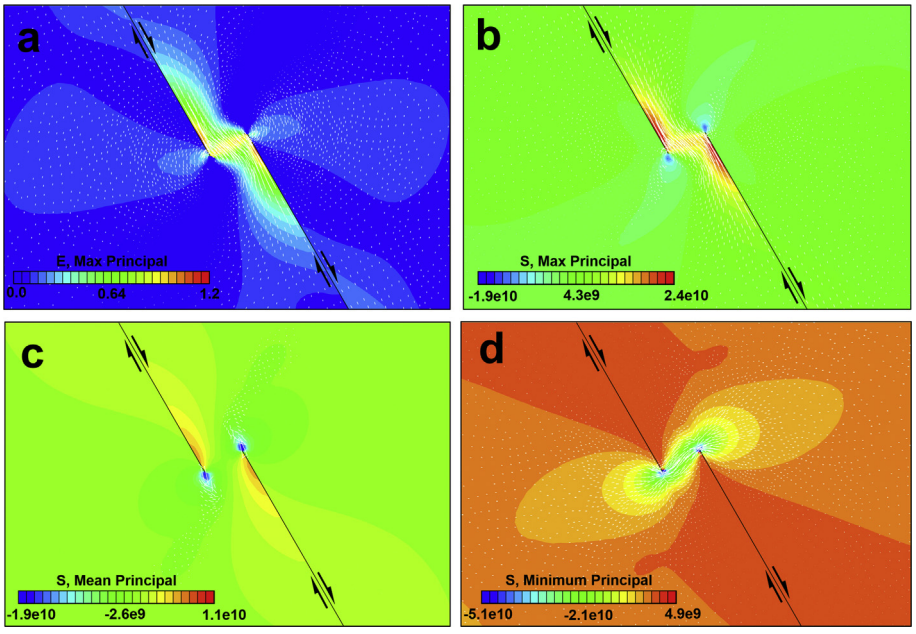

Fig. 18. Model results of **a** maximum principal strain, **b** maximum principal stress, **c** mean principal stress, and **d** minimum principal stress distribution for Kuh-e-Hori transpression zone.

transpression zone between the two left-stepping right-lateral strike-slip fault segments of Esmail-abad and West Neh, SE Iran, shows comparable structural and geomorphological geometries to the neutral step configuration.

Acknowledgements

We would like to express our thanks to Dr. Frantz Maerten for very detailed and constructive reviews and comments that improved the manuscript. This work forms part of the Ph.D. thesis of Seyed Tohid Nabavi at Shahid Beheshti University, Tehran. We thank reviewers Soumyajit Mukherjee and Phaedra Upton for their attentive reading and constructive comments that improved the manuscript. Also, editorial and handling work by Ian Alsop is gratefully acknowledged.

References

Agard, P., Omrani, J., Jolivet, L., Whitechurch, H., Vrielynck, B., Spakman, W., Monie, P., Meyer, B., Wortel, R., 2011. Zagros orogeny: a subduction-dominated process. Geol. Mag. 148, 692–725.

Angiboust, S., Agard, P., De Hoog, J.C.M., Omrani, J., Plunder, A., 2013. Insights on deep, accretionary subduction processes from the Sistan ophiolitic "mélange" (Eastern Iran). Lithos 156–159, 139–158.

Avellone, G., Barchi, M.R., Catalano, R., Morticelli, M.G., Sulli, A., 2010. Interference between shallow and deep-seated structures in the Sicilian fold and thrust belt, Italy. J. Geol. Soc. 167, 109–126.

Aydin, A., Borja, R.I., Eichhubl, P., 2006. Geological and mathematical framework for failure modes in granular rock. J. Struct. Geol. 28 (1), 83–98.

Aydin, A., Nur, A., 1985. The types and role of stepovers in strike-slip tectonics. In: Biddle, K.T., Christie-Blick, N. (Eds.), Strike-slip Deformation, Basin Formation, and Sedimentation, Society of Economic Paleontologists and Mineralogists, vol. 37, pp. 35–44.

Aydin, A., Schultz, R.A., 1990. Effect of mechanical interaction on the development of strike-slip faults with echelon patterns. J. Struct. Geol. 12, 123–129.

Babar, Md, Kaplay, R.D., Mukherjee, S., Kulkarni, P.S., 2017. Evidences of deformation of dykes from central deccan volcanic province, aurangabad, Maharashtra, India. In: Mukherjee, S., Misra, A.A., Calvés, G., Nemčok, M. (Eds.), Tectonics of the Deccan Large Igneous Province, 445. The Geological Society of London, Special Publications. http://dx.doi.org/10.1144/SP445.13 (in press).

Ballato, P., Stockli, D.F., Ghassemi, M.R., Landgraf, A., Strecker, M.R., Hassanzadeh, J., Friedrich, A., Tabatabaei, S.H., 2013. Accommodation of transpressional strain in the Arabia-Eurasia collision zone: new constraints from (U-Th)/He thermochronology in the Alborz mountains, north Iran. Tectonics. http://dx.doi.org/10.1029/2012TC003159.

Barcos, L., Díaz-Azpiroz, M., Balanyá, J.C., Expósito, I., Jiménez-Bonilla, A., Faccenna, C., 2016. Analogue modelling of inclined, brittle-ductile transpression: testing analytical models through natural shear zones (external Betics). Tectonophysics 682, 169–185.

Barreca, G., Maesano, F.E., 2012. Restraining stepover deformation superimposed on a previous fold-and-thrust-belt: a case study from the Mt. Kumeta-Rocca Busambra ridges (western Sicily, Italy). J. Geodyn. 55, 1–17.

Bayet-Goll, A., Monaco, P., Jalili, F., Mahmudy-Gharaie, M.H., 2016. Depositional environments and ichnology of Upper Cretaceous deep-marine deposits in the Sistan Suture Zone, Birjand, Eastern Iran. Cretac. Res. 60, 28–51.

Berberian, M., Jackson, J.A., Qorashi, M., Talebian, M., Khatib, M.M., Priestley, K., 2000. The 1994 Sefidabeh earthquakes in eastern Iran: blind thrusting and bedding-plane slip on a growing anticline, and active tectonics of the Sistan suture zone. Geophys. J. Int. 142, 283–299.

Bertoluzza, L., Perotti, C.R., 1997. A finite-element model of the stress field in strike-slip basins: implications for the Permian tectonics of the Southern Alps (Italy). Tectonophysics 280, 185–197.

Biddle, K.T., Christie-Blick, N., 1985. Glossary – strike-slip deformation, basin formation, and sedimentation. In: Biddle, K.T., Christie-Blick, N. (Eds.), Strike-slip Deformation, Basin Formation, and Sedimentation, Society of Economic Paleontologists and Mineralogists, vol. 37, pp. 375–386.

Blenkinsop, T., 2000. Deformation Microstructures and Mechanisms in Mineral and Rocks. Kluwer Academic Publishers, Dordrecht.

Bourne, S.J., Willemse, E.J.M., 2001. Elastic stress control on the pattern of tensile fracturing around a small fault network at Nash Point, UK. J. Struct. Geol. 23, 1753–1770.

Brankman, C.M., Aydin, A., 2004. Uplift and contractional deformation along a segmented strike-slip fault system: the Gargano Promontary, southern Italy. J. Struct. Geol. 26, 807–824.

Bröcker, M., Fottohi Rad, G., Burgess, R., Theunissen, S., Paderin, I., Rodionov, N., Salimi, Z., 2013. New age constraints for the geodynamic evolution of the Sistan Suture Zone, eastern Iran. Lithos 170–171, 17–34.

Bürgmann, R., Pollard, D.D., 1992. Influence of the state of stress on the brittle-ductile transition in granitic rock: evidence from fault steps in the Sierra Nevada, California. Geology 20, 645–648.

Bürgmann, R., Pollard, D.D., 1994. Strain accommodation about strike-slip fault discontinuities in granitic rock under brittle-ductile conditions. J. Struct. Geol. 16, 1655–1674.

Byerlee, J., 1978. Friction of rocks. Pure Appl. Geophys. 116, 615–626.

Cao, S., Neubauer, F., 2016. Deep crustal expressions of exgumed strike-slip fault systems: shear zone initiation on rheological boundaries. Earth-Science Rev. 162, 155–176.

Camp, V.E., Griffis, R.J., 1982. Character, genesis and tectonic setting of igneous rocks in the Sistan suture zone, eastern Iran. Lithos 3, 221–239.

Channell, J.E.T., Oldow, J.S., Catalano, R., D'Argenio, B., 1990. Paleomagnetically determined rotations in the western Sicilian fold and thrust belt. Tectonics 9, 641–660.

Choi, J.-H., Edwards, P., Ko, K., Kim, T.-S., 2016. Definition and classification of fault damage zones: a review and a new methodological approach. Earth-Science

Rev. 152, 70–87.
Christie-Blick, N., Biddle, K.T., 1985. Deformation and basin formation along strike-slip faults. In: Biddle, K.T., Christie-Blick, N. (Eds.), Strike-slip Deformation, Basin Formation, and Sedimentation, Society of Economic Paleontologists and Mineralogists, vol. 37, pp. 1–35.
Cooke, M.L., Schottenfeld, M.T., Buchanan, S.W., 2013. Evolution of fault efficiency at restraining bends within wet kaolin analog experiments. J. Struct. Geol. 51, 180–192.
Corti, G., Dooley, T.P., 2015. Lithospheric-scale centrifuge models of pull-apart basins. Tectonophysics 664, 154–163.
Crider, J.G., 2001. Oblique slip and the geometry of normal-fault linkage: mechanics ad a case study from the Basin and Range in Oregon. J. Struct. Geol. 23, 1997–2009.
Crider, J.G., 2015. The initiation of brittle faults in crystalline rock. J. Struct. Geol. 77, 159–174.
Cunningham, W.D., Mann, P., 2007. Tectonics of strike-slip restraining and releasing bends. In: Cunningham, W.D., Mann, P. (Eds.), Tectonics of Strike-slip Restraining and Releasing Bends, Geological Society of London, Special Publications, vol. 290, pp. 1–12.
Curtis, M., 1997. Gondwanian age dextral transpression and partial kinematic partitioning within the heritage range, ellsworth mountains, west Antractica. Tectonics 16, 172–181.
Curtis, M., 1999. Structural and kinematic evolution of a Miocene to Recent sinistral restraining bend: the Montejunto massif, Portugal. J. Struct. Geol. 21, 39–54.
Dasgupta, S., Mandal, N., Bose, S., 2015. How far does a ductile shear zone permit transpression? In: Mukherjee, S., Mulchrone, K.F. (Eds.), Ductile Shear Zones: from Micro- to Macro-scales. Wiley, Chichester, pp. 14–29.
Dasgupta, S., Mukherjee, S., 2016. Review on Tectonics of Barmer Rift Basin, India. Tectonic Studies Group 2016 Annual Meeting. University College London, 06–08 January 2016.
Díaz-Azpiroz, M., Barcos, L., Balanyá, J.C., Fernández, C., Exopósito, I., Czeck, D.M., 2014. Applying a general triclinic transpression model to highly partitioned brittle-ductile shear zones: a case study from the Torcal de Antequera massif, external Betics, southern Spain. J. Struct. Geol. 68, 316–336.
Díaz-Azpiroz, M., Brune, S., Leever, K.A., Fernández, C., Czeck, D.M., 2016. Tectonics of oblique plate boundary systems. Tectonophysics 693, 165–170.
Dooley, T.P., McClay, K.R., 1997. Analog modelling of strike-slip pull-apart basins. Am. Assoc. Petroleum Geol. Bull. 81, 804–826.
Dooley, T.P., McClay, K.R., Bonora, M., 1999. 4D evolution of segmented strike-slip fault systems: applications to NW Europe. In: Petroleum Geology of Northwest Europe: Proceedings of the 5th Coference. Geological Society of London, pp. 215–225.
Dooley, T.P., Schreurs, G., 2012. Analogue modelling of intraplate strike-slip tectonics: a review and new experimental results. Tectonophysics 574–575, 1–71.
Favreau, P., Wolf, S., 2009. Theoretical and numerical stress analysis at edges of intersecting faults: application to quasi-static fault propagation modelling. Geophys. J. Int. 179, 733–750.
Fernández, C., Czeck, D.M., Díaz-Azpiroz, M., 2013. Testing the model of oblique transpression with oblique extrusion in two natural cases: steps and consequences. J. Struct. Geol. 54, 85–102.
Flodin, E.A., Aydin, A., 2004. Evolution of a strike-slip fault network, valley of fire state park, southern Nevada. Geol. Soc. Am. Bull. 116, 42–59.
Fossen, H., 2016. Structural Geology, second ed. Cambridge University Press.
Fossen, H., Rotevatn, A., 2016. Fault linkage and relay structures in extensional settings-A review. Earth-Science Rev. 154, 14–28.
Fossen, H., Teyssier, C., Whitney, D.L., 2013. Transtensional folding. J. Struct. Geol. 56, 89–102.
Fossen, H., Tikoff, B., 1993. The deformation matrix for simultaneous simple shearing, pure shearing and volume change, and its application to transpression-transtension tectonics. J. Struct. Geol. 15, 413–422.
Fossen, H., Tikoff, B., 1998. Extended models of transpression and transtension, and application to tectonic settings. In: Holdsworth, R.E., Strachan, R.A., Dewey, J.F. (Eds.), Continental Transpressional and Transtensional Tectonics, Geological Society of London, Special Publications, vol. 135, pp. 15–33.
Fossen, H., Tikoff, B., Teyssier, C., 1994. Strain modelling of transpressional and transtensional deformation. Nor. Geol. Tidsskr. 74, 134–145.
Fotoohi-Rad, G.R., Droop, G.T.R., Burgess, R., 2009. Early Cretaceous exhumation of high-pressure metamorphic rocks of the Sistan Suture Zone, eastern Iran. Geol. J. 44, 104–116.
Frehner, M., 2016a. 3D fold growth in transpression. Tectononphysics 693, 183–196.
Frehner, M., 2016b. Fold axis rotation during transpressional folding: insights from numerical modeling and application to the Zagros Simply Folded Belt. In: GeoMod 2016 Conference, Montpellier, France.
Garfunkel, Z., Ron, H., 1985. Block rotation and deformation by strike-slip faults. 2. The properties of a type of macroscopic discontinuous deformation. J. Geophys. Res. 90 (B10), 8589–8602.
Gölke, M., Cloetingh, S., Fuchs, K., 1994. Finite-element modelling of pull-apart basin formation. Tectonophysics 240, 45–57.
González, D., Pinto, L., Peña, M., Arriagada, C., 2012. 3D deformation in strike-slip systems: analogue modelling and numerical restoration. Andean Geol. 39 (2), 295–316.
Goteti, S.R., 2009. Kinematic and Mechanical Evolution of Relay Zones in Normal Faulted Terranes: Integrating Field Studies in the Rio Grande Rift of North-central New Mexico and Three Dimensional Finite Element Modeling. Unpublished Ph.D. thesis. University of Rochester.
Goteti, S.R., Mitra, G., 2013. Three-dimensional finite-element modeling of fault interactions in rift-scale normal fault systems: implications for the late Cenozoic Rio Grande rift of north-central New Mexico. In: Hudson, M.R., Grauch, V.J.S. (Eds.), New Perspectives on Rio Grande Rift Basins: from Tectonics to Graundwater, Geological Society of America, pp. 157–184. Special Paper 494.
Goteti, S.R., Mitra, G., 2016. Evolution of Relay Zones in Normal Faulted Terranes: Integrating Field Geological Studies with Forward Geomchanical Models. American Rock Mechanics Association.
Granier, T., 1985. Origin, damping and pattern of development of faults in granite. Tectonics 4, 721–737.
Gupta, A., Scholz, C.H., 1998. Utility of elastic models in predicting fault displacement fields. J. Geophys. Res. 103, 823–834.
Gupta, A., Scholz, C.H., 2000. A model of normal fault interaction based on observations and theory. J. Struct. Geol. 22, 865–879.
Ismat, Z., Mitra, G., 2001. Folding by cataclastic flow at shallow crustal levels in the Canyon Range, Sevier orogenic belt, west-central Utah. J. Struct. Geol. 23, 355–378.
Jaeger, J.C., Cook, N.G.W., Zimmerman, R.W., 2007. Fundamentals of Rock Mechanics, fourth ed. Blackwell.
Jones, R.R., Holdsworth, R.E., Clegg, P., McCaffrey, K., Tavarnelli, E., 2004. Inclined transpression. J. Struct. Geol. 26, 1531–1548.
Kaplay, R.D., Babar, M.D., Mukherjee, S., Kumar, T.V., 2017a. Morphotectonic expression of geological structures in eastern part of South East Deccan Volcanic Province (around Nanded, Maharashtra, India). In: Mukherjee, S., Misra, A.A., Calvés, G., Nemčok, M. (Eds.), Tectonics of the Deccan Large Igneous Province, The Geological Society of London, Special Publications, 445. http://dx.doi.org/10.1144/SP445.12 (in press).
Kaplay, R.D., Kumar, T.V., Mukherjee, S., Wesanekar, P.R., Babar, Md, Chavn, S., 2017b. Strike-slip (brittle/brittle-ductile) shear from the periphery of south east deccan volcanic province, kinwat, Maharashtra, India. J. Earth Syst. Sci. submitted.
Kattenhorn, S.A., Krant, B., Walker, E.L., Blakeslee, M.W., 2016. Evolution of the hat creek fault system, northern California. In: Krantz, B., Ormand, C., Freeman, B. (Eds.), 3-D Structural Interpretation: Earth, Mind, and Machine, vol. 11. The American Association of Petroleum Geologists Memoir, pp. 121–154.
Kattenhorn, S.A., Pollard, D.D., 1999. Is lithostatic loading important for the slip behavior and evolution of normal faults in the Earth's crust? J. Geophys. Res. 104, 28879–28898.
Keller, J.V.A., Hall, S.H., McClay, K.R., 1997. Shear fracture pattern and microstructural evolution in transpressional fault zones from field and laboratory studies. J. Struct. Geol. 19, 1173–1187.
Kim, Y.-S., Andrew, J.R., Sanderson, D.J., 2000. Damage zones around strike-slip faults systems and strike-slip fault evolution, Crackington, Haven, southwest England. Geoscience J. 4, 53–72.
Kim, Y.-S., Andrew, J.R., Sanderson, D.J., 2001. Reactivated strike-slip faults: examples from north Cornwall, UK. Tectonophysics 340, 173–194.
Kim, Y.-S., Peacock, D.C.P., Sanderson, D.J., 2003. Strike-slip faults and damage zone at Marsalforn, Gozo Island, Malta. J. Struct. Geol. 25, 793–812.
Kim, Y.-S., Peacock, D.C.P., Sanderson, D.J., 2004. Fault damage zones. J. Struct. Geol. 26, 503–517.
Leever, K.A., Gabrielsen, R.H., Sokoutis, D., Willingshofer, E., 2011. The effect of convergence angle on the kinematic evolution of strain partitioning in transpressional brittle wedges: insights from analog modeling and high-resolution digital image analysis. Tectonics 30, TC2013. http://dx.doi.org/10.1029/2010TC002823.
Lejri, M., 2015. Subsurface Stress Inversion Modeling Using Linear Elasticity: Sensitivity Analysis and Applications. Ph.D. thesis. Montpellier University.
Lejri, M., Maerten, F., Maerten, L., Soliva, R., 2015. Paleostress inversion: a multiparametric geomechanical evaluation of the Wallace-Bott assumptions. Tectonophysics 657, 129–143.
Li, Q., Liu, M., Zhang, H., 2009. A 3-D viscoelastoplastic model for simulating long-term slip on non-planar faults. Geophys. J. Int. 176, 293–306.
Lister, G.S., Snoke, A.W., 1984. S-C mylonites. J. Struct. Geol. 6, 617–638.
Long, J.J., Imber, J., 2011. Geological controls on fault relay zone scaling. J. Struct. Geol. 33, 1790–1800.
Lunn, R., Wilson, J., Shipton, Z.K., Moir, H., 2008. Simulating brittle fault growth from linkage of preexisting structures. J. Geophys. Res. B Solid Earth 113, B07403.
Maerten, F., 2010. Geomechanics to Solve Geological Structure Issues: Forward, Inverse and Restoration Modelling. Unpublished Ph.D. thesis. University of Montpellier II.
Maerten, L., Maerten, F., Lejri, M., Gillespie, P., 2016. Geomechanical paleostress inversion using fracture data. J. Struct. Geol. 89, 197–213.
Maerten, L., Gillespie, P., Daniel, J.-M., 2006. 3-D geomechanical modelling for constraint of subseismic fault simulation. Am. Assoc. Petroleum Geol. Bull. 90, 1337–1358.
Maerten, L., Pollard, D.D., Gillespie, P., 2002. Effects of local stress perturbation on secondary fault development. J. Struct. Geol. 24, 145–153.
Mann, P., 2007. Global catalogue, classification and tectonic origins of restraining and releasing bends on active and ancient strike-slip fault systems. In: Cunningham, W.D., Mann, P. (Eds.), Tectonics of Strike-slip Restraining and Releasing Bends, Geological Society of London, Special Publications, vol. 290, pp. 13–142.
Mann, P., Hempton, P.R., Bradley, D.C., Burke, K., 1983. Development of pull-apart basins. J. Geol. 91, 529–554.
Martel, S.J., 1990. Formation of compound strike-slip zones, Mount Abbot

quadrangle, California. J. Struct. Geol. 12, 869–882.
Martel, S.J., Pollard, D.D., Segall, P., 1988. Development of simple strike-slip fault zones, mount abbot quadrangle, sierra Nevada, California. Geol. Soc. Am. Bull. 100, 1451–1465.
McClay, K.R., Bonora, M., 2001. Analog models of restraining stepovers in strike-slip fault systems. Am. Assoc. Petroleum Geol. Bull. 85, 233–260.
Misra, A.A., Banerjee, S., Kundu, N., Mukherjee, B., 2016. Subsidence around oceanic ridges along passive margins: NE Arabian Sea. In: Mukherjee, S., Misra, A.A., Calvés, G., Nemčok, M. (Eds.), Tectonics of the Deccan Large Igneous Province, The Geological Society of London, Special Publications, 445. http://dx.doi.org/10.1144/SP445.10.
Misra, A.A., Bhattacharya, G., Mukherjee, S., Bose, N., 2014. Near N-S paleo-extension in the western Deccan region in India: does it link strike-slip tectonics with India-Seychelles rifting? Int. J. Earth Sci. 103, 1645–1680.
Misra, A.A., Mukherjee, S., 2015. Tectonic Inheritance in Continental Rifts and Passive Margins. Springer briefs in Earth Sciences.
Misra, A.A., Mukherjee, S., 2017a. Atlas of Structural Geological Interpretation from Seismic Images. Wiley & Blackwell (in press-1).
Misra, A.A., Mukherjee, S., 2017b. Dyke-brittle shear rrelationships in the western Deccan strike-slip zone around Mumbai (Maharashtra, India). In: Mukherjee, S., Misra, A.A., Calvés, G., Nemčok, M. (Eds.), Tectonics of the Deccan Large Igneous Province, The Geological Society of London, Special Publications, 445. http://dx.doi.org/10.1144/SP445.4 (in press-2).
Misra, A.A., Sinha, N., Mukherjee, S., 2015. Repeat ridge jumps and microcontinent separation: insights from NE Arabian Sea. Mar. Petroleum Geol. 59, 406–428.
Misra, S., Mandal, N., Dhar, R., Chakraborty, C., 2009. Mechanisms of deformation localization at the tips of shear fractures: findings from analogue experiments and field evidence. J. Geophys. Res. B Solid Earth 114 (4), B04204.
Mohammadi, A., Burg, J.P., Bouilhol, P., Ruh, J., 2016. U-Pb geochronology and geochemistry of Zahedan and Shah Kuh plutons, southeast Iran: implication for closure of the South Sistan suture zone. Lithos 248–251, 293–308.
Monaco, C., De Guidi, G., 2006. Structural evidence for Neogene rotations in the eastern Sicilian fold and thrust belt. J. Struct. Geol. 28, 561–574.
Mukherjee, S., 2010a. Structures in meso- and micro-scale in the sutlej section of the higher himalayan shear zone, Indian Himalaya. e-Terra 7, 1–27.
Mukherjee, S., 2010b. Microstructures of the zanskar shear zone. Earth Sci. India 3, 9–27.
Mukherjee, S., 2011. Mineral fish: their morphological classification, usefulness as shear sense indicators and genesis. Int. J. Earth Sci. 100, 1303–1314.
Mukherjee, S., 2012a. Simple shear is not so simple! Kinematics and shear zones in Newtonian viscous simple shear zones. Geol. Mag. 149, 819–826.
Mukherjee, S., 2012b. Tectonic implications and morphology of trapezoidal mica grains from the Sutlej section of the Higher Himalayan Shear Zone, Indian Himalaya. J. Geol. 120, 575–590.
Mukherjee, S., 2013a. Deformation Microstructures in Rocks. Springer.
Mukherjee, S., 2013b. Higher Himalayan in the Bhagirathi section (NW Himalaya, India): its structures, backthrust and extrusion mechanism by both channel flow and critical taper mechanisms. Int. J. Earth Sci. 102, 1851–1870.
Mukherjee, S., 2014a. Atlas of Shear Zone Structures in Meso-scales. Springer.
Mukherjee, S., 2014b. Kinematic of 'top-to-down' simple shear in a Newtonian Rheology. J. Indian Geophys. Union 18, 245–248.
Mukherjee, S., 2015a. A review on out-of-sequence deformation in the Himalaya. In: Mukherjee, S., Carosi, R., van der Beek, P., Mukherjee, B.K., Robinson, D. (Eds.), Tectonics of the Himalaya, The Geological Society of London, Special Publications, vol. 412, pp. 67–109.
Mukherjee, S., 2015b. Atlas of Structural Geology. Elsevier, Amsterdam.
Mukherjee, S., 2016. Review on symmetric structures in ductile shear zones. Int. J. Earth Sci. http://dx.doi.org/10.1007/s00531-061-1366-4.
Mukherjee, S., Biswas, R., 2014. Kinematics of horizontal simple shear zones of concentric arcs (Taylor Couette flow) with incompressible Newtonian rheology. Int. J. Earth Sci. 103, 597–602.
Mukherjee, S., Biswas, R., 2015. Biviscous horizontal simple shear zones of concentric arcs (Taylor Couette flow) with incompressible Newtonian rheology. In: Mukherjee, S., Mulchrone, K.F. (Eds.), Ductile Shear Zones: from Micro- to Macro-scales. Wiley-Blackwell, Chichester, pp. 59–62.
Mukherjee, S., 2017. Shear heating by translational brittle reverse faulting along a single, sharp and straight fault plane. J. Earth Syst. Sci. http://dx.doi.org/10.1007/s12040-016-0788-5.
Mukherjee, S., Koyi, H.A., 2010a. Higher Himalayan Shear Zone, Sutlej section: structural geology and extrusion mechanism by various combinations of simple shear, pure shear and channel flow in shifting modes. Int. J. Earth Sci. 99, 1267–1303.
Mukherjee, S., Koyi, H.A., 2010b. Higher Himalayan shear zone, Zanskar Indian Himalaya: microstructural studies and extrusion mechanism by a combination of simple shear and channel flow. Int. J. Earth Sci. 99, 1083–1110.
Mukherjee, S., Koyi, H.A., Talbot, C.J., 2012. Implication of channel flow analogue models in extrusion of the Higher Himalayan shear zone with special reference to the out-of-sequence thrusting. Int. J. Earth Sci. 101, 253–272.
Mukherjee, S., Misra, A.A., Calvés, G., Nemčok, M., 2017. Tectonics of the deccan large igneous province: and introduction. In: Mukherjee, S., Misra, A.A., Calvés, G., Nemčok, M. (Eds.), Tectonics of the Deccan Large Igneous Province, The Geological Society of London, Special Publications, 445 (in press).
Mutlu, O., Pollard, D.D., 2008. On the patterns of wing cracks along an outcrop scale flaw: a numerical modelling approach using complementarity. J. Geophys. Res. B Solid Earth 113, B06403.
Nabavi, S.T., Alavi, S.A., Mohammadi, S., Ghassemi, M.R., Shirzaei, M., 2016a. Analysis of transpression within contractional planar fault steps using the finite-element method. In: Geological Society of America Annual Meeting, Abstracts with Programs, 48, 7.
Nabavi, S.T., Díaz-Azpiroz, M., Talbot, C.J., 2016b. Inclined transpression in the neka valley, eastern Alborz, Iran. Int. J. Earth Sci. http://dx.doi.org/10.1007/s00531-016-1388-y.
Nabavi, S.T., Rahimi-Chakdel, A., Khademi, M., 2016c. Structural pattern and emplacement mechanism of the Neka Valley nappe complex, eastern Alborz, Iran. Int. J. Earth Sci. http://dx.doi.org/10.1007/s00531-016-1433-x.
Nemčok, M., Henk, A., Gayer, R.A., Vandycke, S., Hathaway, T.M., 2002. Strike-slip fault bridge fluid pumping mechanism: insights from field-based palaeostress analysis and numerical modelling. J. Struct. Geol. 24, 1885–1901.
Nevitt, J.M., 2015. Fault-related Deformation within the Brittle-ductile Transition: Field Observations, Microstructural Analysis and Mechanical Modelling. Unpublished Ph.D. thesis. Stanford University.
Nevitt, J.M., Pollard, D.D., Warren, J.M., 2014. Evaluation of transtension and transpression within contractional fault steps: comparing kinematic and mechanical models to field data. J. Struct. Geol. 60, 55–69.
Oldow, J.S., Channell, J.E.T., Catalno, R., D'Argenio, B., 1990. Contemporaneous thrusting and large-scale rotations in the western Sicilian fold and thrust belt. Tectonics 9, 661–681.
Parsons, B., Wright, T., Rowe, P., Andrews, J., Jackson, J.A., Walker, R.T., Khatib, M.M., Talebian, M., Bergman, E., Engdhal, E.R., 2006. The 1994 Sefidabeh (eastern Iran) earthquakes revisited: new evidence from satellite radar interferometry and carbonate dating about the growth of an active fold above a blind thrust fault. Geophys. J. Int. 164, 202–217.
Passchier, C.W., Trouw, R.A.J., 2005. Microtectonics. Springer, Berlin.
Peacock, D.C.P., Nixon, C.W., Rotevatn, A., Sanderson, D.J., Zuluaga, L.F., 2016. Glossary of fault and other fracture networks. J. Struct. Geol. 92, 12–29.
Peacock, D.C.P., Sanderson, D.J., 1995. Pull-aparts, shear fractures and pressure solution. Tectonophysics 241, 1–13.
Pennacchioni, G., Mancktelow, N.S., 2013. Initiation and growth of strike-slip faults within intact metagranitoid (Neves area, eastern Alps, Italy). Geol. Soc. Am. Bull. 125 (9–10), 1468–1483.
Perelló, J., Razique, A., Schloderer, J., 2008. The Chagai porphyry copper belt, Baluchistan province, Pakistan. Econ. Geol. 103 (8), 1583–1612.
Philippon, M., Corti, G., 2016. Obliquity along plate boundaries. Tectonophysics 693, 171–182.
Pollard, D.D., Aydin, A., 1988. Progress in understanding jointing over the past century. Geol. Soc. Am. Bull. 100, 1181–1204.
Pollard, D.D., Fletcher, R.C., 2005. Fundamental of Structural Geology. Cambridge University Press.
Pollard, D.D., Segall, P., 1987. Theoretical displacements and stresses near fractures in rocks: with application to faults, joints, veins, dikes, and solution surfaces. In: Atkinson, B.K. (Ed.), Fracture Mechanics of Rocks. Academic Press, London, pp. 277–349.
Renda, P., Tavarnelli, E., Tramutoli, M., Gueguen, E., 2000. Neogene deformations of northern sicily and their implications for the geodynamics of the southern tyrrhenian sea margin. Boll. della Soc. Geol. Ital. 55, 53–59.
Ritz, E., 2013. Mechanical Behavior of Non-planar Faults: Numerical Experiments and Field Observations. Unpublished Ph.D. thesis. Stanford University.
Ritz, E., Pollard, D.D., Ferris, M., 2015. The influence of the geometry on small strike-slip mechanics. J. Struct. Geol. 73, 49–63.
Rodgers, D.A., 1980. Analysis of pull-apart basins development produced by en échelon strike slip faults. In: Balance, P.F., Reading, H.G. (Eds.), Sedimentation in Oblique-slip Mobile Zones, vol. 4. International Association of Sedimentologists, pp. 27–41.
Saccani, E., Delavari, M., Beccaluva, L., Amini, S., 2010. Petrological and geochemical constraints on the origin of the Nehbandan ophiolitic complex (eastern Iran): implication for the evolution of the Sistan Ocean. Lithos 117 (1), 209–228.
Sanderson, D.J., Marchini, W.R.D., 1984. Transpression. J. Struct. Geol. 6, 449–458.
Sarkarinejad, K., 2007. Quantitative finite strain and kinematic flow analyses along the Zagros transpression zone. Iran. Tectonophys. 442, 49–65.
Sarkarinejad, K., Azizi, A., 2008. Slip partitioning and inclined dextral transpression along the Zagros Thrust System, Iran. J. Struct. Geol. 30, 116–136.
Sarkarinejad, K., Partabian, A., Faghih, A., 2013. Variation in the kinematics of deformation along the Zagros inclined transpression zone, Iran: implications for defining a curved inclined transpression zone. J. Struct. Geol. 48, 126–136.
Sarkarinejad, K., Samani, B., Faghih, A., Grasemann, B., Moradipoor, M., 2010. Implication of strain and vorticity of flow analyses to interpret the kinematics of an oblique convergence event (Zagros Mountains, Iran). J. Asian Earth Sci. 38, 34–43.
Schreurs, G., Colletta, B., 2002. Analogue modelling of continental transpression. In: Schellart, W.P., Passchier, C.W. (Eds.), Analogue Modelling of Large-scale Tectonic Processes, Journal of Virtual Explorer, vol. 7, pp. 103–114.
Segall, P., Pollard, D.D., 1980. Mechanics of discontinuous faults. J. Geophys. Res. 85, 4337–4350.
Segall, P., Pollard, D.D., 1983. Nucleation and growth of strike slip faults in granite. J. Geophys. Res. 88, 555–568.
Soliva, R., Maerten, F., Petit, J.-P., Auzias, V., 2010. Field evidences for the role of static friction on fracture orientation in extensional relays along strike-slip faults: comparison with photoelasticity and 3-D numerical modelling. J. Struct. Geol. 32, 1721–1731.
Strijker, G., Beekman, F., Bertotti, G., Luthi, S.M., 2013. FEM analysis of deformation

localization mechanisms in a 3-D fractured medium under rotating compressive stress orientations. Tectonophysics 593, 95–110.
Sylvester, A.G., 1988. Strike-slip faults. Geol. Soc. Am. Bull. 100, 1666–1703.
Tirrul, R., Bell, I.R., Griffis, R.J., Camp, V.E., 1983. The Sistan suture zone of eastern Iran. Geol. Soc. Am. Bull. 94, 134–150.
Turcotte, D.L., Schubert, G., 2014. Geodynamics, third ed. Cambridge University Press.
Upton, P., Craw, D., 2016. Coeval emplacement and orogeny-parallel transport of gold in oblique convergent orogens. Tectonophysics 693, 197–209.
Upton, P., Craw, D., 2014. Extension and gold mineralization in the hanging walls of active convergent continental shear zones. J. Struct. Geol. 64, 135–148.
Upton, P., Koons, P.O., Craw, D., Henderson, M., Enlow, R., 2009. Along-strike differences in the Southern Alps of New Zealand: consequences of inherited variation in rheology. Tectonics 28. http://dx.doi.org/10.1029/2008TC002353.
Upton, P., Koons, P.O., 2007. Three-dimensional geodynamic framework for the Central Southern Alps, New Zealand: integrating geology, geophysics and mechanical observations. In: Okaya, D., Stern, T., Davey, F. (Eds.), A Continental Plate Boundary: Tectonics at South Island, New Zealand. American Geophysical Union, Washington, DC, pp. 253–270.
Walker, R.T., Jackson, J.A., 2004. Active tectonics and late Cenozoic strain distribution in central and eastern Iran. Tectonics 23, TC5010. http://dx.doi.org/10.1029/2003TC001529.
Walker, R.T., Khatib, M.M., 2006. Active faulting in the Birjand region of NE Iran. Tectonics 25, TC4016. http://dx.doi.org/10.1029/2005TC001871.
Westaway, R., 1995. Deformation around stepovers in strike-slip fault zones. J. Struct. Geol. 17, 831–846.
Willemse, E.J.M., Peacock, D.C.P., Aydin, A., 1997. Nucleation and growth of strike-slip faults in limestones from Somerset, U.K. J. Struct. Geol. 19, 1461–1477.
Willemse, E.J.M., Pollard, D.D., 1998. On the orientation and patterns of wing cracks and solution surfaces at the tips of a sliding flaw or fault. J. Geophys. Res. 103, 2427–2438.
Willemse, E.J.M., Pollard, D.D., Aydin, A., 1996. Three-dimensional analyses of slip distributions on normal fault arrays with consequences for fault scaling. J. Struct. Geol. 18, 295–309.
Woodcock, N.H., Fischer, M., 1986. Strike-slip duplexes. J. Struct. Geol. 8, 725–735.
Woodcock, N.H., Schubert, C., 1994. Continental strike-slip tectonics. In: Hancock, P.L. (Ed.), Continental Deformation. Pergamon, Oxford, pp. 251–263.
Zanchi, A., Zanchetta, S., Balini, M., Ghassemi, M.R., 2016. Oblique convergence during the cimmerian collision: evidence from the triassic aghdarband basin, NE Iran. Godwana Res. 38, 149–170.